DIFFUSION OF ELECTRONS BY COHERENT WAVEPACKETS*

V. Fuchs[+], V. Krapchev, A. Ram and A. Bers

PFC/JA-83-26   July 1983

DIFFUSION OF ELECTRONS BY COHERENT WAVEPACKETS

V. Fuchs

Projet Tokamak, Institut de Recherche d'Hydro Québec, Varennes,

Québec, Canada JOL 2PO

and

V. Krapchev, A. Ram, and A. Bers

Plasma Fusion Center, Massachussetts Institute of Technology,

Cambridge, MA 02139, USA

The momentum transfer and velocity diffusion of electrons period-
ically interacting with a coherent longitudinal wavepacket is consid-
ered. Applying the resonance overlap criterion, we establish the thres-
hold for intrinsic stochasticity and the width of the stochastic region
Δv_{stoch} in velocity space. Direct numerical integration of the single-
particle dynamics and an approximate discrete mapping are used to corro-
borate the resonance overlap results and to find the short-and long-term
momentum transfer and diffusion in the field. After the onset of sto-
chasticity, we find a net induced current $j \sim \Delta v_{stoch}$ and in the weak-
field regime (autocorrelation time $\ll$ bounce time) an initial rate of
change of the variance $<\delta v^2>/2t$ equal to the quasilinear-theory diffusion
coefficient. In the strong- field regime momentum transfer and stochas-
ticity persist owing to non-adiabatic transitions between trapped and un-
trapped states as the electron traverses the wavepacket. The diffusion
coefficient substantially deviates from the quasilinear ($\sim E^2$) as well as
from resonance broadening ($\sim E^{3/2}$) scaling, while the scattering in velo-
locity space tends to lose the local, diffusive, nature characteristic of
weak fields.

I. INTRODUCTION

The understanding of electron velocity scattering by waves is intimately related to the phenomenon of stochastic, as opposed to regular, motion in wave-particle interactions, a problem which has been the subject of intense study in the past few years. A number of benchmark works [1-4] have laid the basis for the understanding of weakly perturbed nonlinear oscillators, while others went on to emphasize and analyze the effect of particle motion stochasticity on plasma collective effects such as heating[5-9] and current-drive[10-11], for example. The classical, and probably the best understood nonlinear wave-particle problem is the nonlinear oscillator, perturbed by one single weak wave. Many problems can be reduced to that particular model or to its representation in the form of a discrete map, the so-called standard or Chirikov map.[12]

The problem we propose to study in the present paper-electron motion in a coherent longitudinal wavepacket - finds itself on the extreme opposite side to the "standard" problem, since we are dealing with particle motion in many waves, which are the Fourier components of the wavepacket. Although adding more and more waves to the standard problem makes it, in principle, less and less tractable, in the limit of a very large number of waves we again recover a familiar situation, similar to that encountered in the quasilinear theory.[13] The principal difference here is that we don't have to postulate random phases for the waves. Rather, once the threshold for resonance overlap is exceeded, the effect of the coherent wave system is to induce intrinsic stochasticity[12] and decorrelation from initial data occurs automatically.

The ultimate goal of this study is to understand the momentum transfer and diffusion of electrons cycling around a torus and periodically interacting with a localized wavepacket of travelling electrostatic waves. This situation is encountered in lower-hybrid heating and/or current drive if the conditions are met for the existence of resonance cones. The source of stochasticity and long time-scale scattering effects are the repeated particle-wavepacket interactions at each cycle around the torus. One particular point of interest is to clarify under what conditions a scattering event is local in velocity space (by this we mean that one can determine the effects on a velocity distribution function f by using derivatives no higher than $\partial^2 f/\partial v^2$). Further, if diffusion is taking place, we might ask whether it scales according to quasi-linear theory. We will see that, in broad terms, diffusion occurs under the familiar condition that the field autocorrelation time be much smaller than the particle trapping time, but that in general, this condition falls short of being a complete one, since behavior in velocity space can be mixed: particles might diffuse in one velocity range, but can strongly scatter, or even reflect, in another.

The physical model we adopt as a basis for our study has been discussed before to some extent by Stix[9] in the study of stochastic heating, by Matsuda[10] in the study of stochastic current drive, and by Fuchs et al[11]. We take further steps here in the analytic as well as numerical treatment of the problem, and an important new contribution consists in emphasizing and analyzing the nonuniform nature of velocity-space for the interaction. In particular, we establish the stochastic

threshold, the width of the stochastic region in velocity-space, and the associated induced long-term current and diffusion coefficient as functions of the field amplitude, of the spectrum, and of the electron cycling length. We derive for the interaction an explicit discrete mapping using weakly perturbed particle trajectories for the diffusion regime, and an implicit mapping based on fully perturbed trajectories valid for strong fields. In numerical investigations of the scattering in velocity-space we use a number of tools: standard surface of section plots, phase-space plots, and a new diagnostic we term the "scattering matrix". This last consists in plotting the particle velocities after an interaction with the wavepacket against the particle velocities just before interaction. The resulting plot shows exactly the range of scatter as a function of particle velocity.

The paper is organized as follows. In section II we introduce the model, basic concepts, and the resonance overlap condition. Momentum transfer and current is discussed in section III, and sections IV deals with the mapping that approximates the dynamic problem. Section V discusses velocity-space diffusion, and section VI presents some features of the strong-field regime. Finally, our conclusions make up section VII.

II. BASIC CONCEPTS

We consider the scattering in velocity-space of electrons peri-
odically interacting with a coherent longitudinal wavepacket. The phys-
ical situation in question could be, for example, lower-hybrid current
drive where electrons orbiting around a torus of effective cycling length
ℓ are subjected to repeated interactions with a uni-directional wave

$$E = E_o \cos (\omega t - kx),$$

acting in a limited spatial region of extent 2d (Fig. 1). Since the sys-
tem is periodic with ℓ, the wave-spectrum is discrete. Typically $\ell > d$, so
that the wave k-spectrum is relatively broad, $\Delta k \approx 1/d$, and the wave-
packet is composed of a large number of modes, $N \approx \ell/d$. If, for the sake
of convenience, we center the interaction region at $x = \ell/2$ and assume a
smooth transition to the field-free region, the single-particle dynamics
can be represented by

$$\frac{d^2x}{dt^2} = \frac{eE_o}{m} \, e^{-(x-\ell/2)^2/d^2} \cos(kx-\omega t). \qquad (1)$$

We will work with a normalized form of Eq. (1), such that space (time)
are dimensionless and normalized to the wavenumber k (frequency ω) of the
wave. Velocities are consequently normalized to the central phase
velocity ω/k. We thus have

$$\ddot{x} = \alpha \exp [-\beta(x-\ell/2)^2]\cos(x-t) \equiv a, \qquad (2)$$

where

$$\alpha = \frac{eE_o k}{m\omega^2} = \frac{\omega_b^2}{\omega^2} \,, \quad \beta = \frac{1}{k^2 d^2} = \left(\frac{\Delta k}{k}\right)^2 .$$

ω_b is the particle bounce frequency at the bottom of the potential well formed by the wave cos kx. The acceleration a has the Fourier series representation

$$a = \frac{\alpha}{\ell}\left(\frac{\pi}{\beta}\right)^{\frac{1}{2}} \sum_{m=-M}^{\infty} (-1)^m \exp(-m^2/4\beta M^2) \cos(k_m x - t), \qquad (3)$$

where M is the nearest integer to $\ell/2\pi$, and $k_m = 1 + m/M$. The representation in terms of Fourier modes is useful in a weak field, such that any particular particle is predominantly affected by the Fourier component whose phase-velocity $v_m = 1/k_m$ is the closest to the particle velocity v. This weak-field stationary-phase concept applies under the condition that the field autocorrelation time be much smaller than the particle trapping time. In our particular situation these two time scales have very definite physical meanings. The autocorrelation time, by definition the width of the field autocorrelation function, is $\tau_{ac} \simeq 2/\sqrt{\beta}$, which is simply the transit time of the particle through the wavepacket. It is thus convenient, for our purposes, to define a trapping time $\tau_b = 2\pi/\omega_b = 2\pi/\sqrt{\alpha}$. If $\tau_{ac} \ll \tau_b$, then the particle transits the interaction region before it can perform more than a small portion of a trapped orbit. Thus τ_b is the shortest trapping time scale in the problem; any of the Fourier components has a longer trapping time. The condition $\tau_{ac} \ll \tau_b$ effec-

tively implies that only the nearest Fourier modes contribute to the resonant wave-particle interaction at a point in velocity-space. In effect, this is a condition of weak resonance overlap. A typical overlap situation in our wave-spectrum is illustrated in Fig. 2, where at each position of phase velocity v_m we plotted at the appropriate height (amplitude) the Fourier mode separatrix full width (trapping width)

$$v_m^{(trap)} = 4(A_m/k_m)^{\frac{1}{2}} = 4(a/\ell)^{\frac{1}{2}} (\pi/\beta)^{\frac{1}{4}} k_m^{-\frac{1}{2}} \exp(-\pi^2/8\beta M^2) \quad (4)$$

In this particular example, the amplitude $\alpha = 0.05$ is about 20 times above threshold for stochasticity. The region of connected stochasticity extends from about $v = 0.6$ to $v = 2.3$. The upper stochastic boundary on the streched-out high-velocity side of the spectrum is due to vanishing overlap, whereas the lower boundary is rather due to a rapidly vanishing field on the low-velocity side. The limited extent of primary island overlap seen here is characteristic of a spatially limited wavepacket and is the principal difference between this case and those which are representable by the standard mapping, where the separation between all modes is the same and where primary-island overlap engulfs the entire phase-space.

The stochasticity associated with island overlap is best evidenced in surface of section plots. In our l - periodic configuration we take the surface of section at $x = 0$ (equivalent to any other position outside the interaction region) and we plot the canonically conjugate pair of variables $v^2/2$ versus t (mod 2π). The plot shown in Fig. 3a corresponds to the parameters of Fig. 2 and is actually the plot v versus t(mod 2π), which has the advantage of directly displaying the extent of the stochastic region. The plot is produced with 10 particles all having the same initial velocity $v_o = 0.8$ and initial position $x_o = 0$, but distinguished one from another by different initial times t_o (an equivalent ensemble would be obtained by taking the same times t_o but different positions x_o). As expected, the particles are fairly uniformly distributed within the region of overlap. The primary islands are completely destroyed all the way from the sharply defined lower stochastic boundary up to where overlap vanishes. The upper stochastic boundary is less well defined than the lower one, and typically exhibits a number of islands since the Fourier mode amplitude converges to a non zero value as v increases and resonance overlap ceases. At low velocity the overlap does not end, rather there is no significant field. In contrast to the result of Fig. 3a, we show in Fig. 3b a sub-threshold case of 10 particles launched at the position of a primary island at $v_o = 0.8$. Since the particles are launched with different phases (to), they occupy different trapped orbits, and those near the separatrix develop secondary islands and spread out in velocity, but not enough to reach the trapping region of neighboring primary islands. We stress at this point that we need not be concerned with the problem of formation of secondary islands, since for our purposes primary island overlap gives a simple and sufficiently accurate estimate of the onset and extent of stochasticity.

Turning now to the formulation of the overlap criterion, we refer to Fig. 2 to see that two neighboring islands overlap if

$$v_m - v_m^{(trap)}/2 < v_{m+1} + v_{m+1}^{(trap)}/2, \tag{6}$$

where $v_m = 1/(1+m/M)$ and the trapping width is given by Eq. (4). Upon substitution we obtain the condition

$$\frac{4\alpha\ell}{\pi^2} \left(\frac{\pi}{\beta}\right)^{\frac{1}{2}} > \frac{\exp(\mu^2/2\beta)}{(1+\mu)^3} \equiv f(\mu), \tag{7}$$

for the mode-number $\mu = m/M$ at which overlap starts. The condition (7) yields both the stochasticity threshold, and the extent of the stochastic region as a function of the excitation parameter S,

$$S = \frac{4\alpha\ell}{\pi^2} \left(\frac{\pi}{\beta}\right)^{\frac{1}{2}} . \tag{8}$$

First, noting that the function $f(\mu)$ has a minimum around $\mu=1$ (actually somewhat below $\mu=1$, depending on β), we immediately see that the threshold for onset of stochasticity is

$$S \simeq 1. \tag{9}$$

when $S > 1$, then the equation

$$S = f(\mu) \tag{10}$$

has two solutions, $\mu_{1,2}$, which determine the modes situated at the edges of the stochastic region. The width of the stochastic region is therefore

$$\Delta v_{stoch} = \frac{1}{1+\mu_1} - \frac{1}{1+\mu_2} .$$

(11)

The onset condition (9) as well as the width (11) are in excellent agreement with numerical results using the surface of section method. It is interesting to note that Stix[9] used a different means of finding a threshold condition. He linearized the corresponding discrete mapping around a primary resonance and obtained the standard mapping, for which the threshold for stochasticity is known. The threshold condition thus determined depends on velocity and amplitude of the primary island chosen. Condition (9) indicates that the threshold is a global property of the system.

III. MAPPING

Before we proceed, in the following sections, with the application of the preceding concepts to the analysis of momentum transfer and diffusion, we will derive, in this section, a useful approximate discrete mapping for the dynamic problem (2). The mapping is a valuable analytic tool in the study of scattering in velocity-space, and its use in computations achieves a typically hundred fold improvement in speed over numerical integration of Eq. (2).

By a mapping we understand the iterated first integrals of the equation of motion (2), under some assumption about the particle trajectory appearing in the phase of the acceleration. Let us therefore assume that the particle trajectory is perturbed only weakly in the interaction with the wavepacket and use for now the unperturbed trajectory

$$x = x_n + v_n (t - t_n) \tag{12}$$

to approximate the phase $(x-t)$ in Eq. (2). (Later we will improve this assumption). Here, we can take $x_n = 0$ owing to the ℓ-periodicity of the the system, v_n is the particle initial velocity for the $(n+1)$-st collision with the wavepacket, and t_n is the time at which the particle crosse the location $x = x_n = n\ell$. In the following, we will consistently use v_{in} for v_n, v_{out} for v_{n+1} (Fig.4), keeping in mind that v_{in} is continuously updated upon entering a new interaction cycle. Upon substitution for

t from (12) into (2), and integration with respect to x from 0 to ℓ, we obtain

$$v^2_{out} - v^2_{in} = 2\alpha(\pi/\beta)^{\frac{1}{2}} \exp(-\rho^2_{in}/4\beta) \cos \chi_{in} ,$$ (13)

where

$$\rho_{in} = 1 - 1/v_{in}, \quad \chi_{in} = \rho_{in}\ell/2 - t_{in} .$$ (14)

In deriving (13), we have used $\ell \gg 1/\sqrt{\beta}$, respecting the original limitations on the problem. The mapping is completed by approximating the integral of $\dot{x} = v$ by

$$t_{out} - t_{in} = \ell(1/v_{in} + 1/v_{out})/2 .$$ (15)

Keeping with the weak-field assumption of slightly perturbed orbits, we can write (13) in the alternative form

$$v_{out} - v_{in} = \Delta v = \frac{\alpha}{v_{in}} \left(\frac{\pi}{\beta}\right)^{\frac{1}{2}} \exp(-\rho_{in}^2/4\beta)\cos\chi_{in}$$ (16)

We are now in the position to examine whether the given mapping is consistent with the weak-field condition $\tau_{ac} \ll \tau_b$. The assumption of weakly-perturbed trajectories translates into requiring that $\Delta v \ll v_{in}$. Since from (16),

$$\Delta v \geq \frac{\alpha}{v_{in}} \left(\frac{\pi}{\beta}\right)^{\frac{1}{2}} ,$$ (17)

we see that the condition

$$\frac{\alpha}{v_{in}} \quad \left(\frac{\pi}{\beta}\right)^{\frac{1}{2}} \ll v_{in} \tag{18}$$

must hold true in order that $\Delta v \ll v_{in}$. The inequality (18) can, however, be written as

$$\frac{1}{v_{in}} \left(\frac{\pi\alpha}{\beta}\right)^{\frac{1}{2}} \quad \frac{\alpha}{v_{in}}^{\frac{1}{2}} \ll 1, \tag{19}$$

which is nothing else but

$$\frac{\tau_{ac}}{\tau_b} \quad \frac{v^{(trap)}}{v_{in}} \ll 1. \tag{20}$$

Since for weak fields almost always $v_{in} > v^{(trap)}$, we see that the weak-field condition $\tau_{ac} \ll \tau_b$ is recovered. We also see that the converse statement is true: $\tau_{ac} \ll \tau_b$ implies $\Delta v \ll v_{in}$, which states that the scattering is local in velocity-space, implying further that the long time-scale effect to expect is diffusion.

A further step toward the understanding of the weak-field mapping (13) or (16) consists in showing that the mapping describes the inter- action of a particle with just one resonant Fourier mode at a time. Let us therefore consider the dynamics of a particle weakly interacting with its resonant Fourier mode, i.e. the equation

$$\dot{v} = \frac{\alpha}{\ell} \left(\frac{\pi}{\beta}\right)^{\frac{1}{2}} \quad \exp(-m^2/4\beta M^2) \cos(k_m x - t). \tag{21}$$

Integrating with respect to time over the unperturbed trajectory (12) yields, after some straightforward algebra,

$$\Delta v = \alpha \left(\frac{\pi}{\beta}\right)^{\frac{1}{2}} \exp\left(-\frac{m^2}{4\beta M^2}\right) \frac{2}{\ell\Omega} \sin\left(\frac{\ell\Omega}{2v_{in}}\right) \cos\Psi, \qquad (22)$$

where, with $\chi = k_m (x_n - v_{in}t_{in})$,

$$\Omega = k_m v_{in} - 1, \quad \Psi = \chi + t_0\Omega + \frac{\ell\Omega}{2v_{in}}. \qquad (23)$$

Since presumably $v_{in} \simeq 1/k_m$, we have $\Omega \to 0$, so that further,

$$\Delta v \simeq \frac{\alpha}{v_{in}} \left(\frac{\pi}{\beta}\right)^{\frac{1}{2}} \exp\left(-\frac{m^2}{4\beta M^2}\right) \cos\chi. \qquad (24)$$

Since, however, $m/M = k_m - 1 = 1 - 1/v_{in}$, we see that (24) is indeed equivalent to (16). The result is not surprising since the integration of Eq. (2) over an unperturbed trajectory automatically performs a stationary-phase selection of the resonant mode.

The map (16) shows how a particle experiences less and less acceleration, and is less scattered, as its velocity deviates from the resonant value $v = 1$. As regards the effect of the phase χ_m, after many orbits it can be considered virtually random, so that the sign of Δv will not be biased on its account. The map (16) reproduces the results of numerical integration quite well but breaks down when one begins to

violate the weak-field condition $\tau_{ac} \ll \tau_b$. The mapping then tends to concentrate near the lower stochasticity boundary where the rapidly vanishing acceleration in that region is handled badly. This tendency is documented in Fig. 5, to be compared with the numerical integration result of Fig. 3a. A further limitation of the mapping (16) will become evident from Figs. 6a,b, where Δv is plotted against v_{in}. In this example, as well as in the preceding one, the amplitude α is fairly large, about 20 times the threshold value $\alpha_{th} = 2.19 \times 10^{-3}$, and $\tau_{ac}/\tau_b = 0.22$.

The mapping result, Fig. 6a, is of course symmetric with respect to the line $\Delta v = 0$, whereas the result of numerical integration, Fig. 6b, exhibits a certain degree of skewness, a lack of symmetry about the line $\Delta v = 0$. Evidently then, the map (16) which for any v_{in} allows Δv and $-\Delta v$ to occur with equal probability is incapable of describing a long-term evolution having a nonvanishing ensemble-average, $\langle \Delta v \rangle = 0$.

The two shortcomings of the mapping (16) that we have just discussed originate in the assumption of unperturbed trajectories. We will now remove this restriction. Instead of using Eq. (12) to approximate the phase, we perform the integration in two parts, accounting for the acceleration effect on phases by using the two- step trajectories

$$x = v_{in} (t - t_{in}), \quad 0 < x \; 0 < \ell/2$$

$$(25)$$

$$x = \ell/2 + v_{out} (t - t_{in} - \ell/2v_{in}), \quad \ell/2 < x < \ell.$$

We thus obtain the mapping in implicit form

$$v_{out}^2 - v_{in}^2 = \alpha \left(\frac{\pi}{\beta}\right)^{\frac{1}{2}} (e^{-z_{in}^2} + e^{-z_{out}^2}) \cos\chi_{in}$$

$$\qquad\qquad (26)$$

$$+ \frac{2\alpha}{\sqrt{\beta}} [D(z_{in}) - D(z_{out})] \sin\chi_{in},$$

where $z = (1 - 1/v)/2\sqrt{\beta}$ and $D(z)$ is Dawson's integral

$$D(z) = e^{-z^2} \int_0^z e^{t^2} dt. \qquad\qquad (27)$$

To order α^2, a small-pertubation assumption now gives, upon Taylor - expanding around v_{in},

$$\Delta v = \frac{\alpha}{v_{in}} \left(\frac{\pi}{\beta}\right)^{\frac{1}{2}} e^{-z_{in}^2} \cos\chi_{in}$$

$$- \frac{\alpha^2 \pi}{2\beta v_{in}^3} (1 + \frac{\rho_{in}}{\beta v_{in}}) \exp(-\frac{\rho_{in}^2}{2\beta}) \cos^2\chi_{in}$$

$$- \frac{\sqrt{\pi}}{4} \frac{\alpha^2}{\beta^{3/2} v_{in}^4} e^{-z_{in}^2} \sin 2\chi_{in} [1 - z_{in} D(z_{in})]. \qquad (28)$$

The first term on the right hand side is the first approximation (16), whereas the remaining terms represent the effect of a weakly perturbed orbit.

The mapping (28) is much better approximation than is (16). It tends much less to concentrate particles near the lower stochastic boundary. This is clearly shown by the surface of section plot in Fig. 7a, produced from Eq. (28) under the same conditions as Fig. 5. Also,

the Δv versus v_{in} plot in Fig. 7b now reproduces the skewness seen in Fig. 6b (with a slight excess at the highest Δv). This is very good considering the strength of the field in this case. The skewness of mapping (28) yields a nonvanishing ensemble-average v , namely,

$$\langle \Delta v \rangle_{\chi} = - \frac{\alpha^2 \pi}{4\beta v_{in}^3} \ (1 + \frac{\rho_{in}}{\beta v_{in}}) \ \exp(-\frac{\rho_{in}^2}{2\beta}) \ . \tag{29}$$

This is an important property of the mapping, as can be fully appreciated by realizing that $\langle \Delta v \rangle_{\chi}$ is the local measure of momentum transfer between the waves and the particles. Equation (29) essentially tells us that particles below resonance ($v_{in} < 1$) gain momentum, while particles above resonance lose momentum. We will show later, in section V, that $\langle \Delta v \rangle$ in Eq. (29) is related to the friction coefficient $\partial D/\partial v$.

IV. MOMENTUM TRANSFER, CURRENT

Results of the previous section show that there is a net non-vanishing average acceleration acting on resonant particles. The long-time-scale effect is thus sustained momentum transfer in a distribution of electrons spread almost uniformly within the stochastic region given by Eqs. (10) and (11). We are now interested in the net total momentum transferred in the interaction. For the sake of definiteness, let us therefore imagine the field interacting with a Maxwellian plasma, in a region of velocities much larger then the thermal velocity. Then most of the electrons which are being pulled into the resonant region Δv_{stoch} originate at the lower stochasticity boundary and, as a result, a net total momentum is being continuously transferred from the field to the particles. In order to calculate this momentum transfer, no details of the acceleration process are required if the time-asymptotic behavior is known.

Let us represent the situation just described by a resonant distribution of electrons which evolves in time under the influence of the field, from on initial δ - function to a time-asymptotic form which vanishes outside Δv_{stoch}, but is nonvanishing and uniform inside that interval, situated between v_1 and v_2, say. The net current produced in the transition from the initial (fo) to the time-asymptotic state (f) is, by definition,

$$j = \int v (f - fo) \, dv, \tag{30}$$

subject to the constraint of particle conservation

$$\int (f_0 - f) \, dv = 0. \tag{31}$$

Hence

$$f = 1/\Delta v_{stoch} \quad , \tag{32}$$

and since $f_0(v) = \delta(v - v_0)$, we obtain

$$j = \frac{1}{2} (v_1 + v_2 - 2v_0). \tag{33}$$

If the particles originate at $v_0 = v_1$, the current is maximum,

$$j = \frac{1}{2} \Delta v_{stoch}. \tag{34}$$

The value of Δv_{stoch} is plotted in Fig. 8 together with the numerically determined ensemble average $<v - v_0>$. In the numerical investigations, typically 100 particles are all launched at an initial velocity v_0 inside the stochastic region near the lower boundary v_1, but having different initial phases (t_0 or x_0). The ensemble is allowed to repeatedly collide with the wavepacket until $<v>$ reaches a steady-state. The net current $<v - v_0>$ is seen to be in excellent agreement with the expected value (34). Also plotted in Fig. 8 are the lower and upper stochasticity

boundaries. The values $v_{1\ 2}$ were calculated independently using the overlap criterion and surface of sections plots with excellent agreement between the two methods.

As shown in Fig. 8 the behavior of j is somewhat different just above stochastic threshold and well above threshold. Well above stochastic threshold the induced current increases with electric field and with β. This is to be expected since the upper limit v_2 increases with β for a given field. Since the field threshold for onset of stochasticity increases with spectral width (since the wave energy is spread over more modes) increasing β when near threshold will reduce the current . These results explain those of Matsuda[10] who found that electrons transiting a "well-defined" resonance cone (larger β) will carry a larger current than those interacting with a "spread-out" one.

V. DIFFUSION

If electron-wavepacket collisions are more frequent than particle-particle collisions and the electron trajectories are only weakly perturbed in individual electron-wavepacket collisions, then on a time scale longer than the autocorrelation time, the evolution of the resonant particle distribution function f can be conveniently described by the Fokker-Planck equation[14]

$$\frac{\partial f}{\partial t} = -\frac{\partial (\nu f)}{\partial v} + \frac{\partial^2 (Df)}{\partial v^2} .$$ (35)

If the diffusion coefficient D and the friction coefficient ν are simply related as

$$\nu = \frac{\partial D}{\partial v} ,$$ (36)

then Eq. (35) can be written in the form

$$\frac{\partial f}{\partial t} = \frac{\partial}{\partial v} \left(D \frac{\partial f}{\partial v} \right) ,$$ (37)

known as the quasilinear diffusion equation[13]. This simple model of the effect of particle scattering, requiring just one coefficient, D(v), is a strong motivation to formulate the D representing a particular wave-particle interaction. The standard practice in the weak-field regime is to calculate D(v) from the decay in time of the fluctuating field auto-correlation function as seen by unperturbed electrons at velocity v. This gives the so-called quasilinear diffusion coefficient. Successive

iterations of the procedure[15] with perturbed trajectories leads to the resonance broadening theory result[16]. There have also been attempts to formulate a diffusion coefficient in the strong-field, trapping, regime. For example, Flynn[17] supports, in numerical investigations, the notion of a "trapping" diffusion coefficient as formulated by Dupree[16], while Graham and Fejer[18] contest such an idea.

The diffusion we are studying is limited in velocity space to the stochastic region. If the step Δv that the particle takes at every crossing of the interaction domain is much smaller than the width of the stochastic region, the diffusion coefficient depends on the velocity of the particle between interactions. Therefore, for short times (a few drift times ℓ/v), the relevant quantity is $D(v)$. In this respect, because of the intrinsic stochasticity the interaction of electrons with a coherent wavepacket resembles the one with a random phase wavepacket for which agreement with quasilinear theory was established by Doveil and Gresillon[15]. After many interactions the particle has explored the whole stochastic domain and then the meaningfull quantity is a diffusion coefficient averaged over velocities in the stochastic region, $D(v)$. $D(v)$ describes the long-time behavior of the system.

Let us begin with the standard quasilinear (QL) formulae. By definition,

$$D_{QL} = \lim_{t \to \infty} \frac{d}{dt} \frac{\langle \delta v^2 \rangle}{2} \tag{38}$$

where

$$\delta v = \int_0^t a(\tau)d\tau. \tag{39}$$

$a(t)$ is given in Eq. (2), the integration is performed along unperturbed trajectories (12), and the pointed brackets signify ensemble-averaging. We obtain

$$D_{QL}(v) = \frac{\alpha^2 \pi}{4\beta \ell v} \exp\left[-\frac{(1-1/v)^2}{2\beta}\right] \tag{40}$$

The same result is immediately obtained using the mapping (16), from which, by definition,

$$D(v_{in}) = \frac{<\Delta v^2>_X}{2\tau_{drift}}, \tag{41}$$

where $\tau_{drift} = \ell/v_{in}$ is the electron drift time between two interaction events, and the averaging is performed over the phase. As regards the associated friction coefficient, we have, from (36) and (40),

$$\nu_{QL} = -\frac{\alpha^2 \pi}{4\beta \ell v^2} \left(1 + \frac{\rho}{\beta v}\right) \exp\left(-\frac{\rho^2}{2\beta}\right). \tag{42}$$

In order to recover this result from the discrete mapping, we take the perturbed trajectory result (29) and we note that, by definition[14] $v = <\Delta v>/t_o$, where the appropriate time-scale t_o is here the electron drift time ℓ/v_{in}.

To what extent the system will really exhibit quasilinear behavior in the sense given by the preceding coefficients D and ν, can be verified by numerical experiments involving the evolution of the averages $\langle\Delta v\rangle$ and $\langle\Delta v^2\rangle$ in a large ensemble of particles. Then, by definition[14],

$$\nu = \frac{\langle\Delta v\rangle}{t_o} , \quad D = \frac{\langle\Delta v^2\rangle}{2t_o} \tag{43}$$

We proceed as follows. Typically we launch a group of 1000 particles all having the same velocity v_o, but distinguished one from another by different initial times or positions. We let the ensemble transit the wavepacket just once and evaluate (the initially vanishing) $\Delta v = \langle v-v_o\rangle$ and $\Delta v^2 = \langle v^2\rangle - \langle v\rangle^2$, where

$$\langle v\rangle = \frac{1}{N}\sum v_n , \quad \langle v^2\rangle = \frac{1}{N}\sum v_n^2 . \tag{44}$$

We repeat this procedure for a number of initial velocities v_o within the stochastic region, so that we obtain ν and D as a function of v_o. This is because in one transit through the wavepacket the particle loses memory of its initial phase, while at the same time retaining memory of the initial velocity condition. The results for one particular choice of α and β are shown in Fig. 9. Although $\tau_{ac} = 0.22\,\tau_b$ which is just about at the limit of the weak-field region, we see that the quasilinear results hold very well indeed. Serious deviations from quasilinear predictions develop, however, when the ratio τ_{ac}/τ_b approaches unity. A good appreciation of this tendency can be obtained from the

global results of Fig. 10, where D is plotted as a function of α. Each of the Figs 10a,b show 4 curves, two of which represent computational data (D and $\bar{D}$), the other two being theory (D_{QL} and $\bar{D}_{QL}$). D and D_{QL} are local (velocity-dependent) diffusion coefficients, whereas $\bar{D}$ and $\bar{D}_{QL}$ are average quantities. The corresponding pairs ($\bar{D}$, $\bar{D}_{QL}$) and (D, D_{QL}) agree in the weak-field regime, but otherwise the deviation of numerical from quasilinear results is substantial. The scaling of D and $\bar{D}$ with α in the strong-field regime also considerably deviates from that expected on the basis of resonance-broadening theory[16] ($\alpha^3/^2$). We will return to the strong-field case in the next section, but now a few words about the significance of the average quantities $\bar{D}$ and $\bar{D}_{QL}$ are in order.

We were motivated to introduce $\bar{D}$ and $\bar{D}_{QL}$ in order to describe the long-time-scale diffusion. In our case, since the accessible region of velocity-space is bounded, the variance $<\Delta v^2>$ eventually saturates as a function of time and $<\Delta v^2>/2t$ vanishes, although individual particles continue to be scattered. In order to define a diffusion coefficient for long times, we follow one or more particles through a large number of successive interactions with the wavepacket and we define D_t as the average over the number of cycles N_c,

$$\bar{D} = \frac{1}{N_c} \Sigma \quad \frac{\Delta v^2}{2t_c} , \quad t_c = \ell/v_{in},$$
(45)

where $\Delta v = v_{out} - v_{in}$, taken at each interaction event. After many interactions, the particle has lost memory of the initial conditions, and, in particular, $\bar{D}$ tends to a value independent of v_o. This is demonstrated in Fig. 11, where $\bar{D}$ is calculated for 6 values of v_o inside the stochastic region. Hence, $\bar{D}$ represents a true ensemble as well as velocity-space average.

To describe theoretically the behavior of the system for long times (many interactions) we define the average

$$\bar{D}_{QL} = \langle \frac{\Delta v^2}{2t_{drift}} \rangle_{\chi, v_{in}} = \langle D_{QL} \rangle_{v_{in}} , \qquad (46)$$

where Δv is given by (16) and the average is taken with respect to the ensemble (χ) and velocity-space (v_{in}). Since v_{in} is presumably spread uniformly over the stochastic region situated between, say, v_1 and v_2, we have

$$\bar{D}_{QL} = \frac{\alpha^2 \pi}{4\beta \ell} \frac{1}{v_2 - v_1} \int_{v_1}^{v_2} \frac{e^{-(1-1/v)^2/2\beta}}{v} dv. \qquad (47)$$

The interval (v_1, v_2) is situated around the resonant value $v = 1$, and excludes the point $v = 0$, so that $\bar{D}$ can be approximated by

$$\bar{D}_{QL} \simeq \frac{\alpha^2 \pi}{4\beta \ell} \quad \frac{1}{v_2 - v_1} \quad \int_{1-1/v_1}^{1-1/v_2} e^{-z^2/2\beta} \, dz. \tag{48}$$

In this form, $\bar{D}_{QL}$ is easily related to the rms field. Referring to the Fourier series (3), we see that

$$a_{rms}^2 = \frac{1}{2} \frac{\alpha^2 \pi}{\beta \ell^2} \quad \sum_m \quad e^{-m^2/2\beta M^2}. \tag{49}$$

If we keep in (49) only the overlapping modes and pass to the limit of an integral, we obtain

$$a_{rms}^2 (\text{stoch}) = \frac{1}{2} \frac{\alpha^2 \pi}{\beta \ell^2} \quad M \int_{\mu_1}^{\mu_2} \quad e^{-z^2/2\beta} \, dz, \tag{50}$$

where $\mu = m/M$. Recalling that $M \simeq \ell/2\pi$ and that $\mu = 1 - 1/v$, we have further

$$a_{rms}^2 (\text{stoch}) = \frac{\alpha^2}{4\ell\beta} \quad \int_{1-1/v_1}^{1-1/v_2} \quad e^{-z^2/2\beta} \, dz, \tag{51}$$

whence it follows that D_v can be written in the form

$$\bar{D}_{QL} = a_{rms}^2 (\text{stoch}) \quad \tau_{ac} (\text{stoch}), \tag{52}$$

with

$$\tau_{ac} (\text{stoch}) = \pi/(v_2 - v_1) \tag{53}$$

We stress that the autocorrelation time (53), has the appropriate form[16] for a spectrum broadened over an interval spanning from v_1 to v_2. The equivalence of the velocity-space average $\bar{D}_{QL}$ and the time-average $\bar{D}$ in the weak-field regime is evident from Fig. 10.

To sum up, distinction must be made between short-term and long-term temporal effects. On a short time scale of the order of one scattering event ($t \simeq \ell/v$) in the weak-field regime, diffusion is quasisilinear. On a long time scale, as particles fill the accessible bounded region of velocity-space, diffusion in terms of the rate of change of the velocity variance ceases, but the diffusion coefficient $\bar{D}$ defined by Eq. (45) tends to the same non zero limit for all particles in the stochastic region. Thus, $\bar{D}$ and its theory counterpart $\bar{D}_{QL}$, formulated in terms of the stochastic part of the spectrum, are the appropriate long-time diffusion coefficients.

VI. STRONG-FIELD REGIME

In this section we present material, mostly numerical results, that we consider essential to the understanding of the strong-field interaction. let us recall that by the strong-field regime we understand conditions violating the inequality $\tau_{ac} \ll \tau_b$, so that scattering is no longer necessarily local in velocity space. In addition to the change in magnitude, there is also a change in the typical character of particle trajectory pertubations. The rms weak-field effect is now superseded by trapped-particle-orbit effects.

We wish to immediately point out that there exists, in the strong-field case, an upper limit of allowable field strengths, imposed by the lack of self-consistency in our model. This limit is $\alpha \approx 1$, which guarantees that no particles from the bulk of the distribution are affected by the wavepacket. Under these conditions, we can assume that the wave maintained by the bulk particles remains unchanged, and we study the nonlinear dynamics it induces on the resonant particles. No electrostatic one-dimensional spatially modulated wave-exists in a plasma when $\alpha v_{phase}/v_{thermal} > 1.7.$[19] Some results of computations with $\alpha \geq 1$ will, however, be shown in order to stress certain features of the strong-field regime. The two characteristic strong-field effects are here the ponderomotive force acting on low-velocity nonresonant particles, and non-adiabatic crossings of a separatrix as a resonant particle is first captured and subsequently escapes from a trapped orbit in the wavepacket.

The most important class of particles affected by the pondero-motive force are those which reside around $v = 0$, i.e. the bulk parti-cles. Their trajectories are very weakly perturbed and can be written in the form

$$x(t) = x_0(t) + \tilde{x}(t), \tag{54}$$

where $x_0(t)$ $[\tilde{x}(t)]$ gives the slow (fast) time-dependence. The equation of motion for the slowly varying part is

$$\ddot{x}_0 = \langle \alpha e^{-\beta(x_0 + \tilde{x} - \ell/2)^2} \cos(x_0 + \tilde{x} - t) \rangle, \tag{55}$$

where we average over t. If $\alpha \ll 1$, then we find to order α

$$\tilde{x} \simeq - \alpha e^{-\beta(x_0 - \ell/2)^2} \cos(x_0 - t) \qquad \ll 1, \tag{56}$$

which leads to

$$\ddot{x}_0 = - \frac{\alpha^2}{4} \frac{d}{dx_0} e^{-2\beta(x_0 - \ell/2)^2}. \tag{57}$$

The ponderomotive potential is therefore

$$\phi_{pond} = \frac{\alpha^2}{4} e^{-2\beta(x_0 - \ell/2)^2}, \tag{58}$$

and particles incoming at velocities less than $v_{in} = \alpha/\sqrt{2}$ will be reflected. Such a particle is seen, for example, in the surface of section plot, Fig. 12, where 9 particles where launched within the stochastic region and one outside at $v_o = 0.2$. The nonresonant particle obviously bounces back and forth on a constant energy surface.

The resonant interaction, in contrast to the ponderomotive reflection, leads to a very complicated velocity-space structure. The surface of section plot in Fig. 12a belies this fact to a large extent, since the distribution of velocities appears fairly uniform. The first, quite obvious, difference between the strong-field case of Fig. 12 and a typical weak-field one, shown in Fig. 3a for example, is the appearance in Fig. 12a of a stochastic band in the region of negative velocities. This indicates that some of the resonant particles can now be reflected, and that this reflection is non-adiabatic, in contrast to the ponderomotive case. The extent of the negative stochastic region as a function of α is indicated in Fig. 8 by the dashed-dotted line, mirrored onto the positive side for the sake of convenience. Another, rather fundamental, difference between the strong-and weak-field cases consists in the perception by a particle of Fourier modes. Fig. 12b shows the resonance overlap diagram for the example of Fig. 12a. The overlap is so strong that a resonant particle sees a large number of Fourier modes at the same time. As a result, the usual picture of stochasticity associated with resonance overlap breaks down, and the stochasticity observed in Fig. 12a must be of different origin. In effect, the particle now sees the wavepacket as a whole, rather than its individual Fourier components. How then does a particle become stochastic? The answer is that if the

particle is trapped, once inside the wavepacket, it had to cross a separatrix, and will have to do so once again upon exiting from the interaction region. The transitions from trapped to untrapped states and vice-versa are, in general, non-adiabatic[20]. The existence of trapped particle orbits in the wavepacket can be detected using stroboscopic and direct v versus x phase-space plots. A sample of these is shown in Fig. 13. In contrast to a surface of section plot, where the state of a particle is recorded just once during a cycle around the torus, the motion is now monitored everywhere including the interaction region. The v versus x plot (Fig. 13a) shows 5 successive transits of the interaction region, and immediately indicates the following characteristics of the motion. First, the existence of an elliptic point situated at $v = 1$, second, the non-adiabicity of the interaction ($v_{out} \neq v_{in}$, in general), and finally the expected dependence of a trapped orbit on initial phase and velocity. In the stroboscopic plots, the velocity and corresponding position are recorded in succession at times separated by the natural period 2π, for a large number of transits and/or particles, and thus give a comprehensive phase-space picture. The first thing to realize is that essentially all particle orbits are recorded in the process, and in particular also trapped orbits if such exist. The envelope of trapped orbits is the separatrix. At peak amplitude the separatrix should span the velocity interval $1 \pm 2\sqrt{\alpha}$, which is exactly what we see in both Figs. 13b,c. For the very strong-amplitude case of $\alpha = 4$ reflections occur owing to the extension of trapped orbits into the region of negative velocities.

particle is trapped, once inside the wavepacket, it had to cross a separatrix, and will have to do so once again upon leaving the interaction region. The transitions from trapped to untrapped states and vice-versa are, in general, non-adiabatic[20]. The existence of trapped particle orbits in the wavepacket can be detected using stroboscopic and direct v versus x phase-space plots. A sample of these is shown in Fig. 13. In contrast to a surface of section plot, where the state of a particle is recorded just once during a cycle around the torus, the motion is now monitored everywhere including the interaction region. The v versus x plot (Fig. 13a) shows 5 successive transits of the interaction region, and immediately indicates the following characteristics of the motion. First, the existence of an elliptic point situated at $v = 1$, second, the non-adiabicity of the interaction ($v_{out} \neq v_{in}$, in general), and finally the expected dependence of a trapped orbit on initial phase and velocity. In the stroboscopic plots, the velocity and corresponding position are recorded in succession at times separated by the natural period 2π, for a large number of transits and/or particles, and thus give a comprehensive phase-space picture. The first thing to realize is that essentially all particle orbits are recorded in the process, and in particular also trapped orbits if such exist. The envelope of trapped orbits is the separatrix. At peak amplitude the separatrix should span the velocity interval $1 \pm 2\sqrt{\alpha}$, which is exactly what we see in both Figs. 13b,c. For the very strong-amplitude case of $\alpha = 4$ reflections occur owing to the extension of trapped orbits into the region of negative velocities.

The phase-space plots of the preceding discussion are useful diagnostics
for probing the nature of particle orbits, but for information about the
structure in velocity-space of particle scattering we have to go to Δv
versus v_{in} plots, such as in Fig. 6b, for example. We prefer an alterna-
tive representation, in terms of v_{out} versus v_{in}, i.e. "scattering
matrices". In the scattering matrix, the indication of interaction is a
departure from the diagonal, i.e. from the identity line $v_{out} = v_{in}$. The
sequence in Fig. 14 shows the progress in the magnitude of velocity-
scattering as the amplitude α is increased from $\alpha = 0.1$ to $\alpha = 0.5$ and
then $\alpha = 4$. For $\alpha = 0.1$, which is the limit of the weak-field regime
when $\beta = 0.1$, we see that everywhere $\Delta v \ll v_{in}$, indicating that diffusion
is still a good approximation of the scattering in that case. For
$\alpha = 0.5$ scattering is stronger and some structure has developed in the
scattering pattern. At $\alpha = 4$ velocity-space has become very non-uniform:
reflections can occur in one region of velocity-space, while diffusion
persists elsewhere. Such a mixed phase-space is typical of wide spectra,
characterized by a strechted-out high velocity side so that weak
resonance overlap is possible there. Fig. 15 shows the difference, in
this respect, between wide and narrow spectra.

In our next example of Fig. 16, showing the extremely intricate
structure of scattering in the deeply trapped regime of $\tau_{ac}/\tau_b = 4.5$, we
in one case (a) produce the plot by following one single particle for
5000 collisions with the wavepacket, whereas in the other (b) we launch
5000 particles spread uniformly between $v_{in} = -2$ and $v_{in} = 4$ and let the
ensemble collide with the wavepacket just once. The reason for doing so
is two-fold. First we are thus able to demonstrate the two distinct

classes of nonresonant particles. To the first class belong particles which are virtually unperturbed by the field and hence occupy the identity line $v_{out} = v_{in}$. The other class is composed of particles which are adiabatically reflected by the ponderomotive force. In the plot these form the segment perpendicular to the identity line. The non-adiabatically reflected particles originating from trapped orbits are seen to form a diffuse extension of the ponderomotive branch. The second reason has to do with the general question of time-and-ensemble-averages. Fig. 16 directly demonstrates that it makes no difference to the scattering pattern in what manner an interval dv_{in} is populated. Also obvious is now the fact that the system requires no more than one interaction time to fully establish its scattering characteristics.

We will close this section with a few remarks about momentum transfer and diffusion in strong fields. First, going back to Fig. 8, we note that the current j persists for large α, and so does its correlation with Δv_{stoch}. In Fig. 8b we observe, however, a change in the scaling of j with α, which we attribute to the dominance of the wavepacket trapping width over the proper spectrum width, as documented for example in Fig. 12b. The non-adiabatically reflected particles populating the band delineated by the dashed-dotted line act as a counter-propagating beam, but the pre-dominance of transiting particles caused by the bias in the direction of the travelling wave, quarantees a net current in that direction. A wider wave-spectrum will support a larger current because the correspondingly larger number of Fourier modes on the stretched-out high velocity side of the spectrum will form a wider region of overlap.

In regard to diffusion, the preceding results indicate its limited validity as a means of describing the particle-velocity scattering in the strong-field regime. If we are prepared, though, to sacrifice local features in favor of a long-time global description of the scattering process, it suffices to recognize that the interaction remains non-adiabatic and that a certain region of velocity-space is ultimately almost uniformly populated regardless of particle initial conditions. Hence a long-time, global, diffusive description survives in the form of the average quantity $\bar{D}$, defined by Eq. (45) and computed in Fig. 10. We right away note the substantial change in scaling with α that $\bar{D}$ experiences as the strong-field regime takes over. Such a change in scaling can only be explained through the effect of a new velocity step-size, replacing the weak-field expression $\Delta v \simeq a_{rms}\, \tau_{ac} \sim \alpha/\sqrt{\beta}$. A crude estimate of the new scaling can be obtained as follows. Knowing that the velocity jump under strong-field conditions is related to the width of a trapped particle orbit, we have, on the average, $\Delta v \simeq \sqrt{\alpha}$. Consequently, $D \simeq \alpha/2\ell$, having taken a particle-wavepacket "collision" time $\ell/v \simeq \ell$. Let us now compare this result with the numerically established $\bar{D}$. In addition to the strong field data of Fig. 10, we show additional results in Fig. 17, which collects all the strong field $\bar{D}$ of Figs 10a and 10b, and also includes $\bar{D}$ for $\beta = 0.001$ (not shown previously). In terms of magnitude, $\alpha/2\ell$ falls below $\bar{D}$ by about a factor of ten. Moreover, the scaling is seen to depend on β .In conclusion, more work is required in order to interpret the strong-field results, the key point being an analysis of action non-conservation during separatrix crossing.

VII. <u>CONCLUSION</u>

Having analysed the scattering in velocity-space of electrons repeatedly interacting with a discrete spectrum of coherent waves, whose extent is limited in configuration-, wavenumber-, and velocity-space, we offer the following general picture of the interaction. Above a certain threshold, which depends on field strength, spectrum width and electron cycling length, the interaction is non-adiabatic and particle motion is stochastic within a bounded, not necessarily simply-connected, region of velocity-space. The nature of the interaction, and also the source of stochasticity, depends on the ratio of two basic time scales in the problem: the particle transit time through the wavepacket which is also the autocorrelation time τ_{ac}, and the particle bounce time τ_b in the wavepacket.

When $\tau_{ac} \ll \tau_b$, the particle-velocity scattering is everywhere local in velocity-space and the diffusion approximation holds. In this, weak-field, regime the particle-wavepacket interaction is characterized by weak resonance overlap, such that during one cycling time an electron interacts exclusively with just one or two Fourier modes. The wandering, or diffusion, through a region of non-zero extent in velocity space is then a long-time-scale phenomenon induced by the nonlinear effect of resonance overlap during many interactions with the wavepacket. This long-term diffusion must be distinguished from the short-term, local, effect, which is quasilinear in nature, by virtue of intrinsic stochasticity having automatically replaced random phase waves. The quasi-

linearity of the short-term interaction is shown directly by comparing

the numerical short-term evolution of the velocity mean and variance with

the quasilinear-theory friction and diffusion coefficients. Analyti-

cally, a discrete mapping representing the interaction with weakly per-

turbed particle-trajectories also yields the exact quasilinear results,

and is easily generalized to an implicit form including the effect of

strongly perturbed trajectories. The long-term diffusion coefficient is

obtained by averaging the quasilinear expression over the stochastic

region of velocity-space. This average proves to be equivalent to the

time average taken for any resonant particle.

While the weak-field interaction can be generally characterized

by the effect of a rms field on a resonant particle acting for a period

of the autocorrelation time, the strong-field interaction is, in con-

trast, characterized by the existence of trapped particle orbits, the

bounce time now being smaller than the autocorrelation time. In addi-

tion, strong resonance overlap can occur, so that a resonant electron can

percieve many Fourier modes at a time. In other words, on the short

timescale a particle can no longer be thought of as interacting with

individual field components, but rather, its interaction with the wave-

packet as a whole must be considered. For wide spectra, such that $\Delta k/k$

is not much less then unity, the situation becomes very complicated,

since strong overlap in the region around the phase-velocity combines

with the effect of weak overlap on the stretched-out branch of the

spectrum, $v_{ph} < v$. Such a mixed velocity-space causes particles to weakly scatter in one region, but to suffer large displacements, even reflection in another. Either way, the observed long-term effect of the interaction is to scatter the particles almost uniformly throughout a bounded region in velocity-space, indicating a generally non-adiabatic process. For the particles that are temporarily trapped in the wave-packet the source of non-adiabaticity are the two crossings of a separa-trix upon entering and leaving the wavepacket. Long-term momentum transfer and diffusion therefore persist in the strong-field regime. The numerically determined long-term diffusion coefficient deviates substantially from its weak-field counterpart in terms of scaling with the field strength E. Depending on the spectrum width, the scaling is somewhere between $E^{\frac{1}{2}}$ and E.

A more detailed study of the strong-field regime, based on the analysis of action non-conservation during separatrix crossing is in preparation.

ACKNOWLEDGMENTS

REFERENCES

1) G.M. Zaslavskii and N.N. Filonenko, Sov. Phys. JETP $\underline{25}$, 851 (1968).

2) G.M. Zaslavskii and B.V. Chirikov, Sov. Phys. Usp. $\underline{14}$, 549 (1972).

3) A.B. Rechester and T.H. Stix, Phys. Rev. $\underline{A19}$ 1656 (1979).

4) M.N. Rosenbluth, R.Z. Sagdeev, J.B. Taylor, and G.M. Zaslavskii, Nucl. Fusion $\underline{6}$, 297 (1966).

5) G.R. Smith and A.N. Kaufman, Phys. Rev. Lett. $\underline{34}$, 1613 (1975), also Phys. Fluids $\underline{21}$, 2230 (1978).

6) C.F.F. Karney and A. Bers, Phys, Rev. Lett. $\underline{39}$, 550 (1977).

7) C.F.F. Karney, Phys. Fluids $\underline{21}$, 1584 (1978); $\underline{22}$, 2188 (1979).

8) J.Y. Hsu, K. Matsuda, M.S. Chu, and T.H. Jensen, Phys. Rev. Lett. $\underline{43}$, 203 (1979).

9) T.H. Stix, in Proceedings of the Third Symposium on Plasma Heating in Toroidal Devices, edited by F. Sindoni (Editrice Compositori, Bologna, 1976), p. 159.

10) K. Matsuda, in Proceedings of the Fourth Topical Conference of Radio-Frequency Heating in Plasmas, Austin, Texas, 1981, paper B10; also Stochastic Current Drive by Plasma Waves, General Atomic Company Report GA-A16303, July 1981.

11) V. Fuchs, V. Krapchev, A. Ram, and A. Bers, in Proceedings of the Fifth Topical Conference on Radio-Frequency Heating in Plasmas, Madison, Wisconsin, 1983, paper B-L.1.

12) B.V. Chirikov, Phys. Reports 52, 263 (1979).

13) N.A. Krall and A.W. Trivelpiece, Principles of Plasma Physics (Mc Graw-Hill, New-York, 1973), Chap. 10.

14) S. Ichimaru, Basic Principals of Plasma Physics: A Statistical Approach (W.A. Benjamin, Inc., Reading, Massachusetts, 1973), Chap. 10.

15) F. Doveil and D. Gresillon, Phys. Fluids 25, 1396 (1982).

16) T.H. Dupree, Phys. Fluids, 9, 1773 (1966).

17) R.W. Flynn, Phys, Fluids 14, 956 (1971).

18) K.N. Graham and J.A. Fejer, Phys. Fluids 19, 1054 (1976).

19) V. Krapchev and A. Ram, Phys. Rev. A22, 1229 (1980).

20) R.E. Aamodt and E.F. Jaeger, Phys. Fluids 17, 1386 (1974).

43.

FIGURES CAPTIONS

Fig. 1: Geometric configuration of wave-particle interaction.

Fig. 2: Spectrum in velocity-space. The full separatrix width of a Fourier mode is indicated at the position of its phase-velocity and amplitude.

Fig. 3: Surface of section plot, velocity versus phase, taken half-way between two interactions. (a) particles launched at $v_o = 0.08$ are monitored for 500 cycles through the wave-packet.
(b) Sub-threshold conditions, otherwise as per (a).

Fig. 4: Configuration for mapping. v_{out}, t_{out} and $x = 0$ are initial conditions for new cycle.

Fig. 5: Surface of section plot from the mapping (16), at conditions of Fig. 3a.

Fig. 6: Δv versus v_{in}. (a) From the mapping (16). (b) From numerical integration.

Fig. 7: (a) Surface of section plot from the mapping (28) at conditions of Fig. 3a and 5. (b) Δv versus v_{in} from the mapping (28), conditions as per (a).

Fig. 8: The lower (v_1) and upper (v_2) stochasticity boundaries and the long-term current j, as functions of the field strength α. The dashed-dotted line indicates the width of the stochastic region of negative velocities (reflected particles). (a) $\beta = 0.1$, (b) $\beta = 0.01$.

Fig. 9: The short-term diffusion (D) and friction (dD/dv_0) coefficients as a function of particle velocity. The solid lines are from quasilinear theory, the points are from numerical integrations.

Fig. 10: The diffusion coefficient as a function of field strength α. D_{QL} is the quasilinear value at $v = 0.8$, D is from numerical integrations of an ensemble of particles, $\bar{D}_{QL}$ is velocity-space averaged D_{QL}, and $\bar{D}$ is the time-average from numerical integration of one particle. (a) $\beta = 0.1$, (b) $\beta = 0.01$.

Fig. 11: The particle diffusion coefficient $\bar{D}$ as a function of the number of successive cycles, for 6 values of particle initial velocity in the stochastic region.

Fig. 12: (a) Surface of section plot. 9 particles launched at $v_0 = 0.8$ and 1 particle launched outside the stochastic region at $v_0 = 0.2$; 500 cycles. (b) Corresponding resonance overlap diagram.

Fig. 13: Phase-space plots, velocity versus position. (a) 5 successive transits of a resonant particle through the wavepacket. (b) Stroboscopic plot. v and x are recorded at $t = t_0 + 2\pi n$, $n = 0,1,...,$ for 5000 cycles; $\alpha = 0.4$. (c) Stroboscopic plot, $\alpha = 4$.

Fig. 14: Scattering diagrams, v_{out} versus v_{in}; $\beta = 0.1$. (a) $\alpha = 0.1$, (b) $\alpha = 0.5$, (c) $\alpha = 4$.

Fig. 15: Resonance overlap diagrams for $\alpha = 0.4$. (a) Wide spectrum,

$\beta = 0.1$. (b) Narrow spectrum, $\beta = 0.01$.

Fig. 16: Scattering diagrams. (a) One particle, 5000 cycles.

(b) 5000 particles distributed uniformly between $v_{in} = -2$ and

4, one cycle.

Fig. 17: The diffusion coefficient $\bar{D}$ as a function of α in the strong-

field regime for $\beta = 0.1$, 0.01 and 0.001. Different point-

types correspond to different particle initial conditions.

Electron cycling length, ℓ

Interaction region, 2d

$\mathscr{v}_{out}$

$\mathscr{v}_{in}$

$E_0 \, e^{-x^2/d^2} \cos(kx - \omega t)$
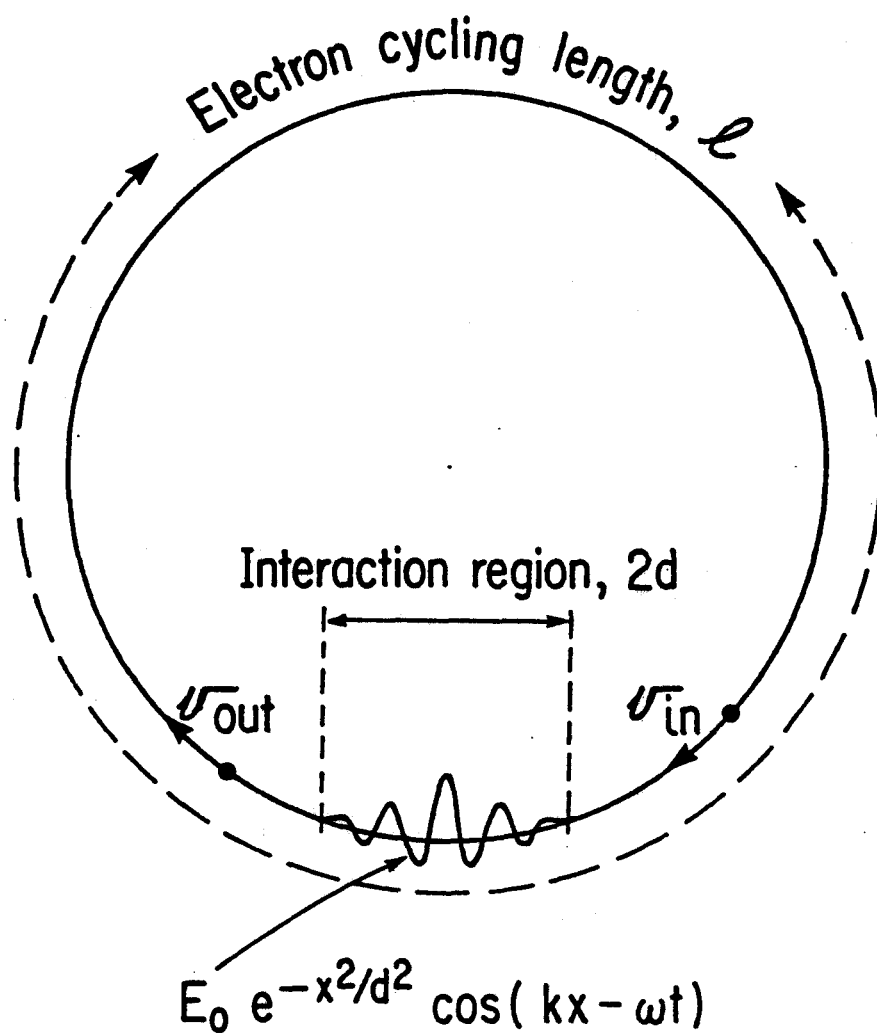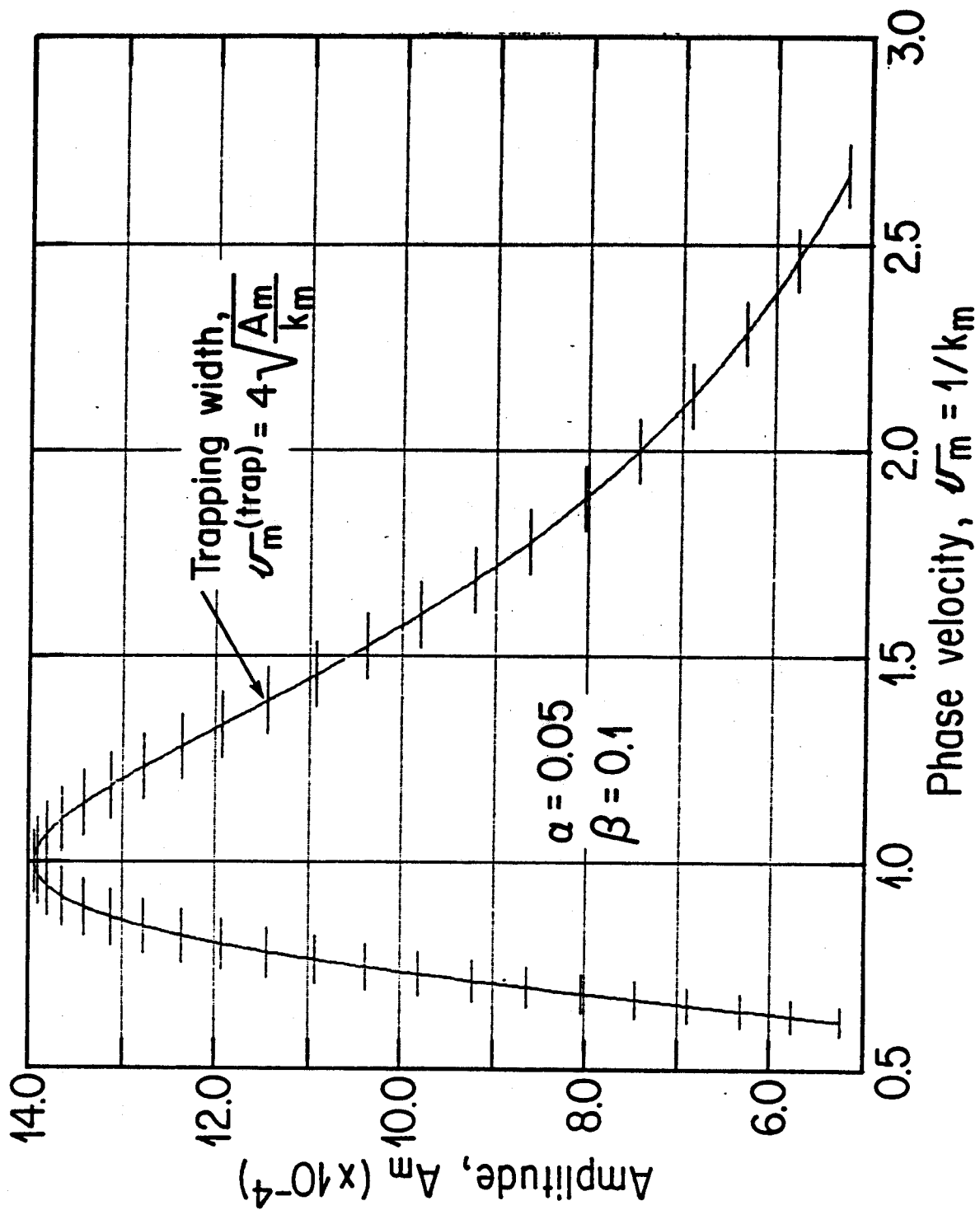
Fig. 1

Fig. 2
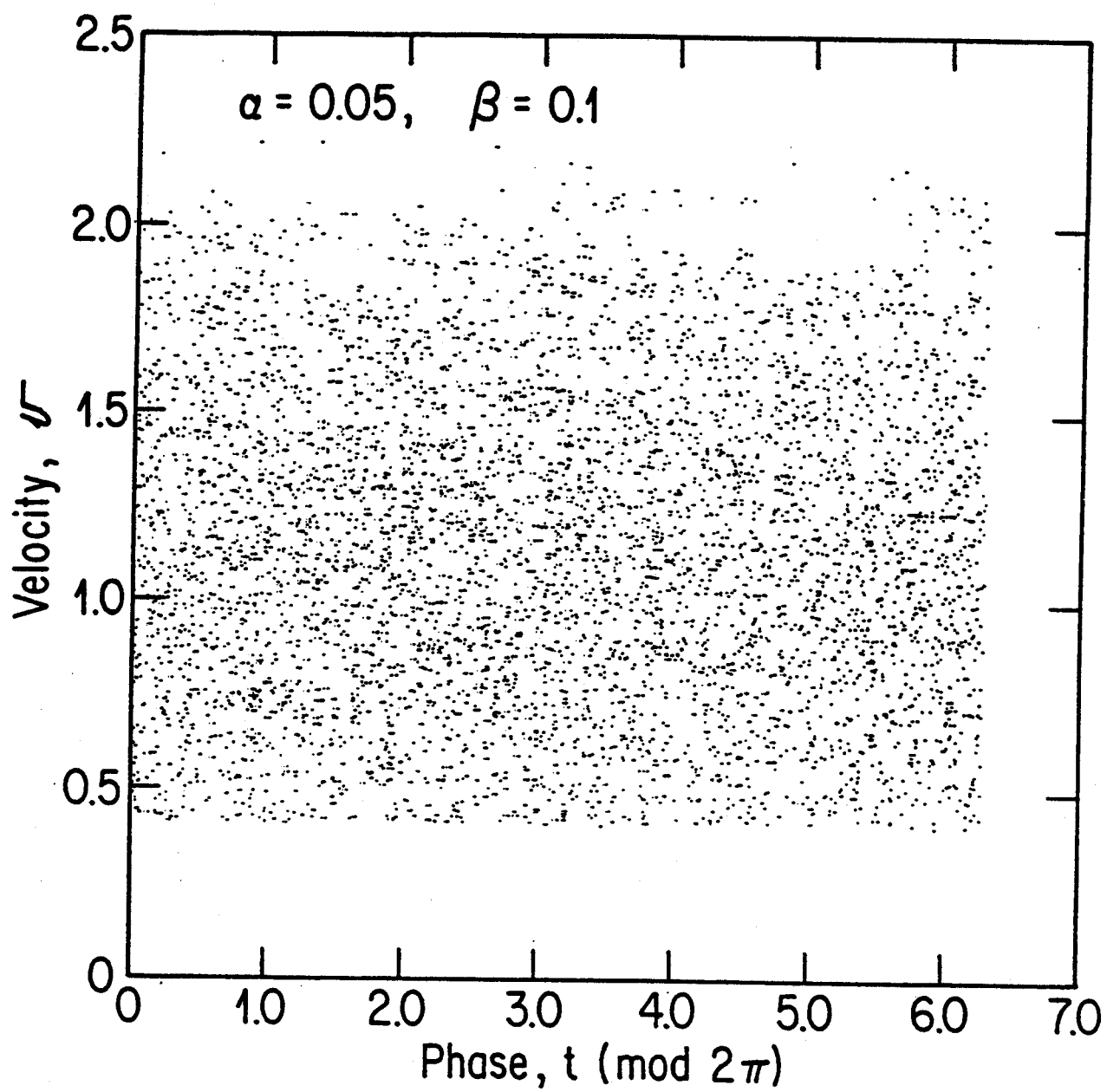
Fig. 3a

Fig. 3b

Fig. 4

Fig. 5

α = 0.05
β = 0.1
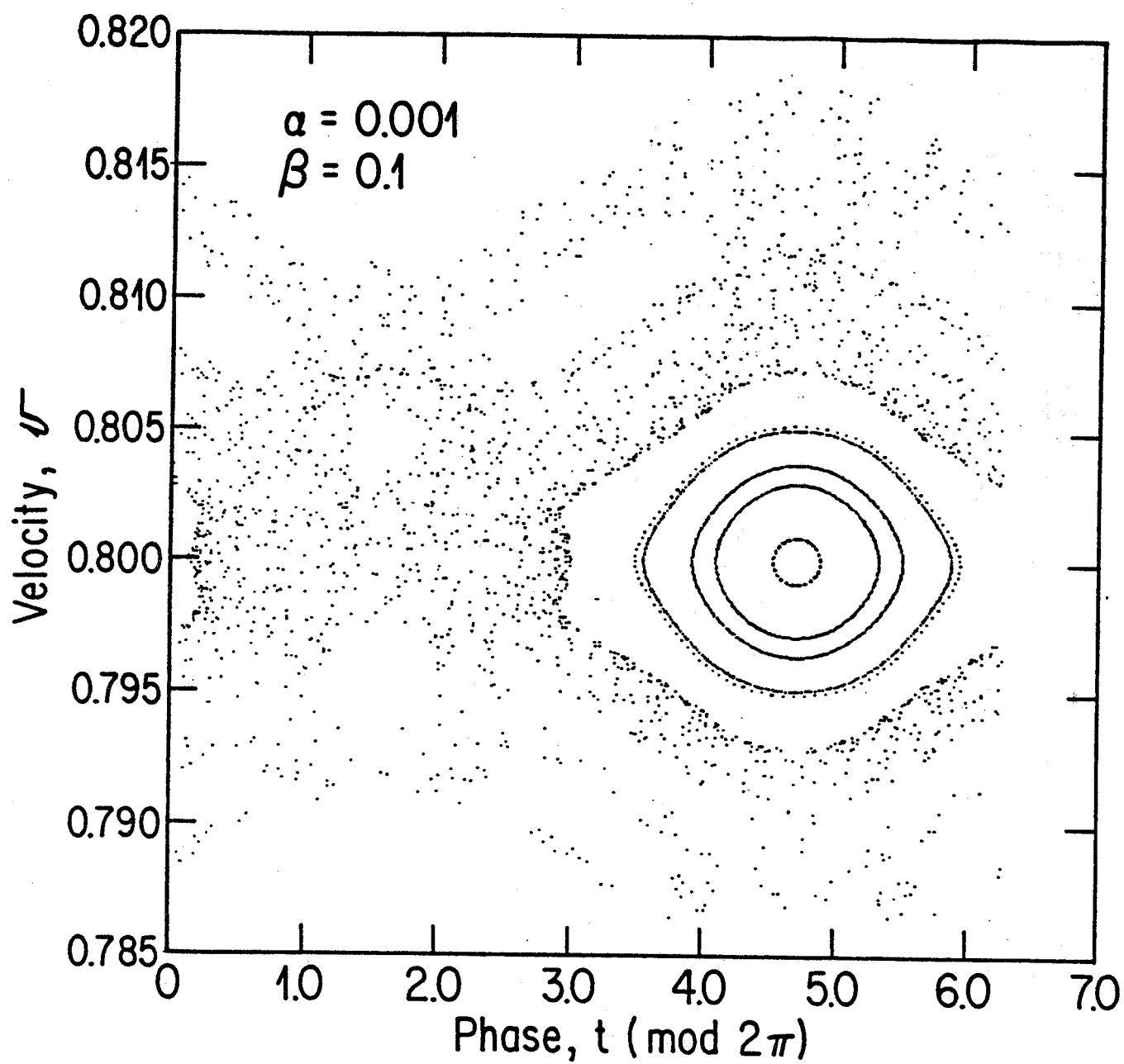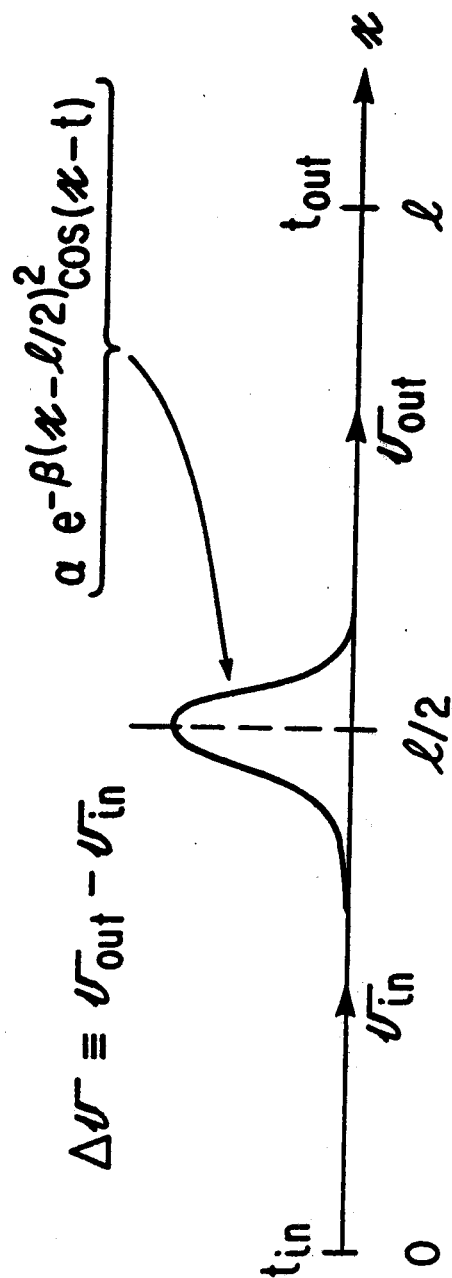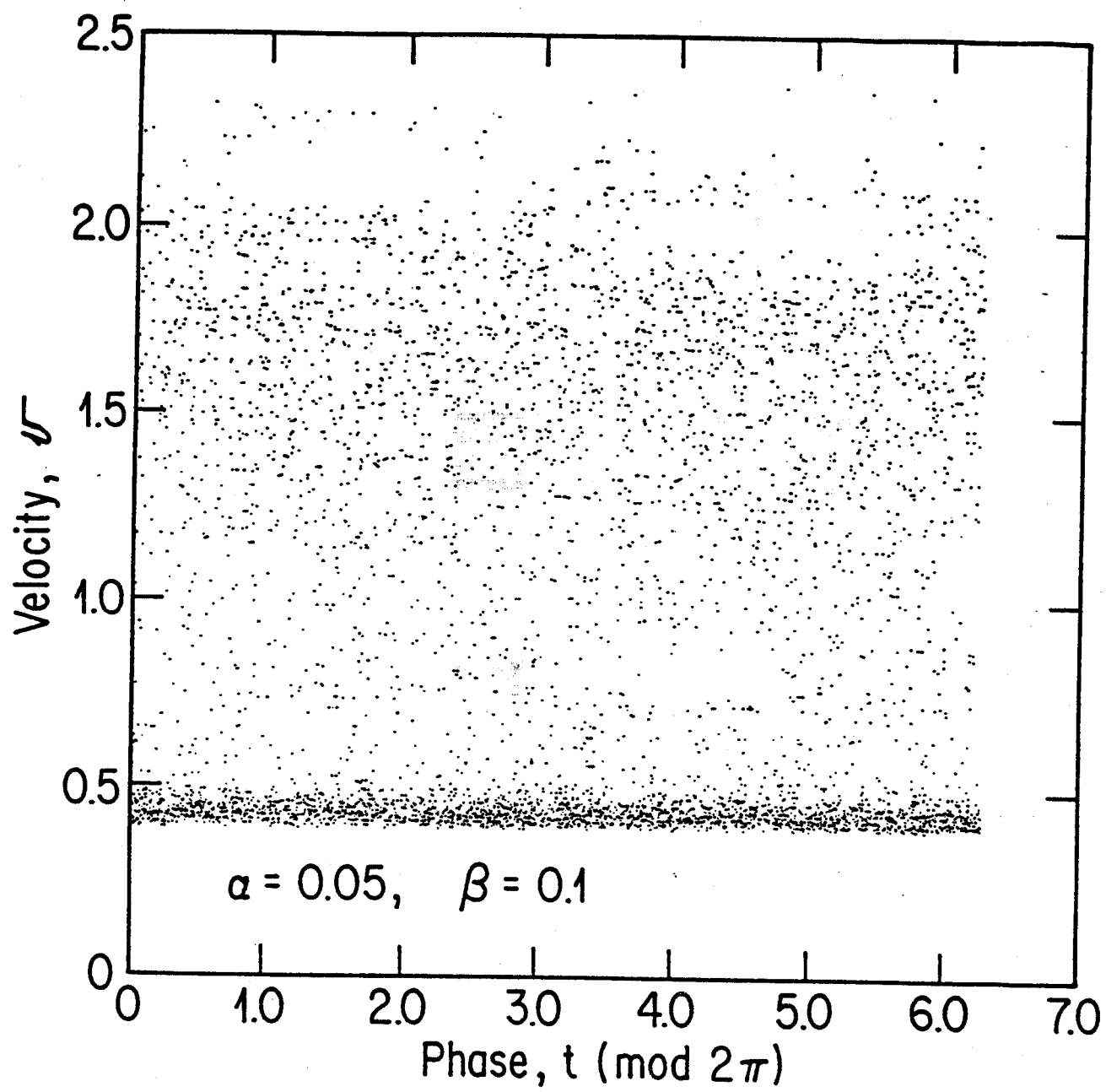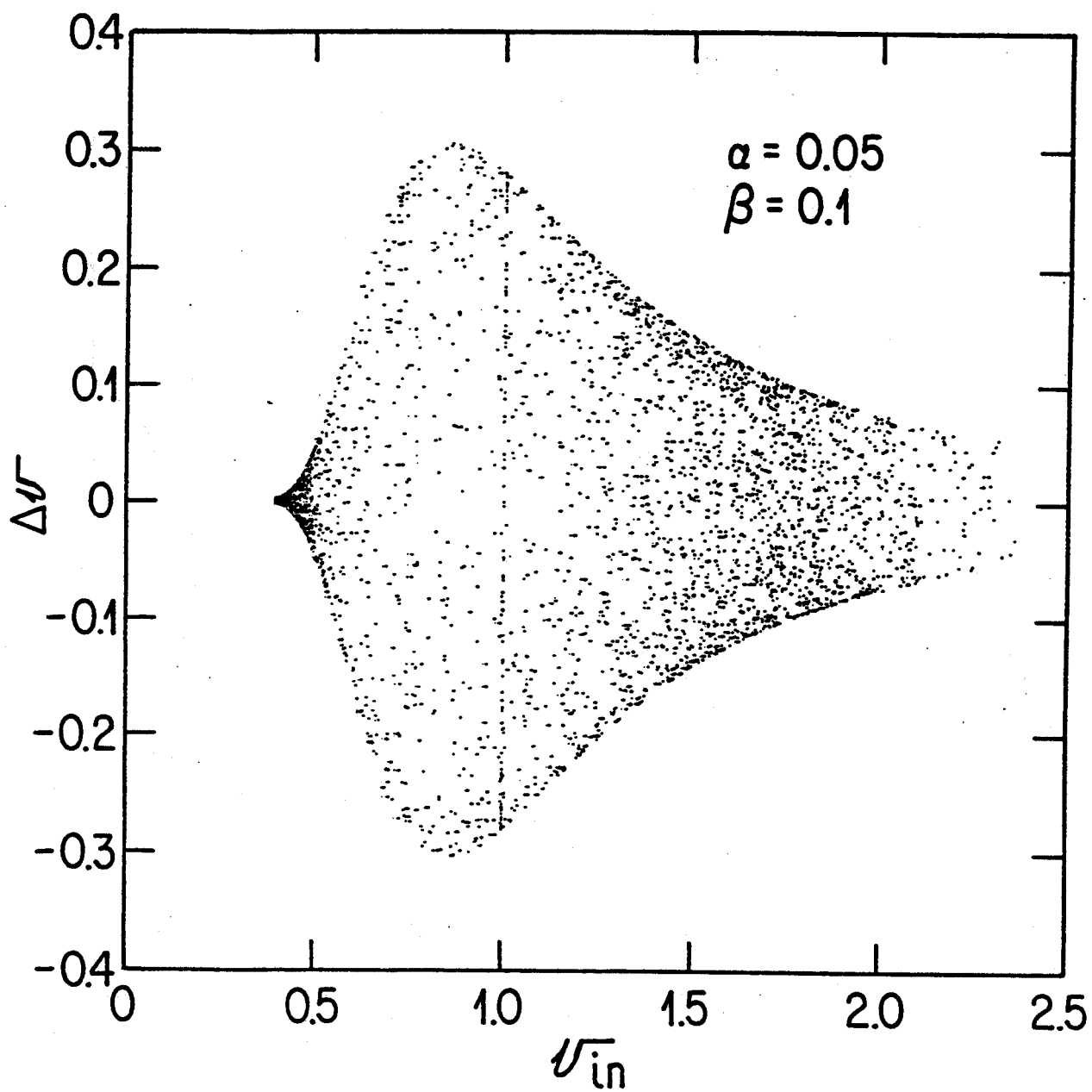
Fig. 6a
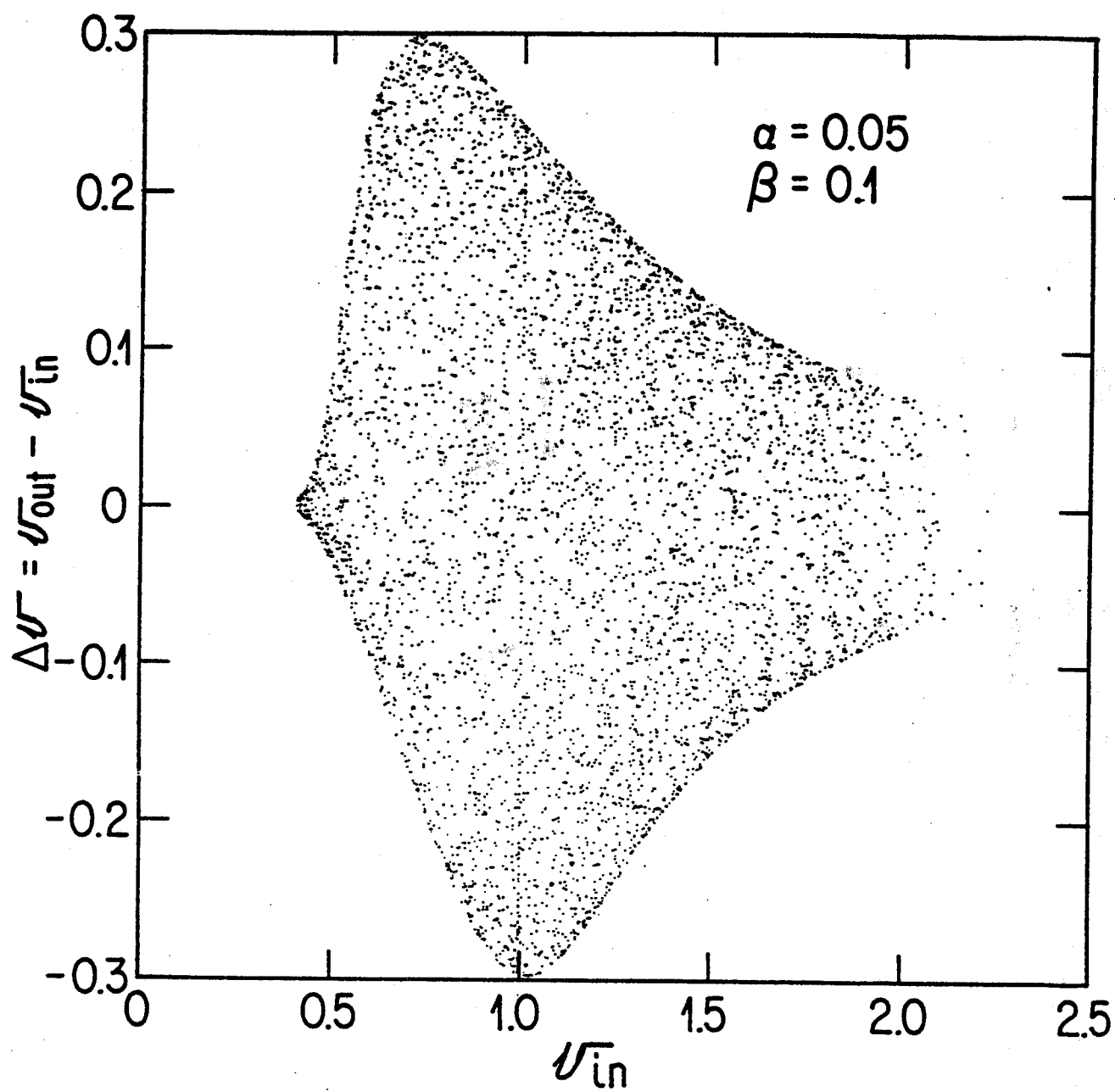
Fig. 6b
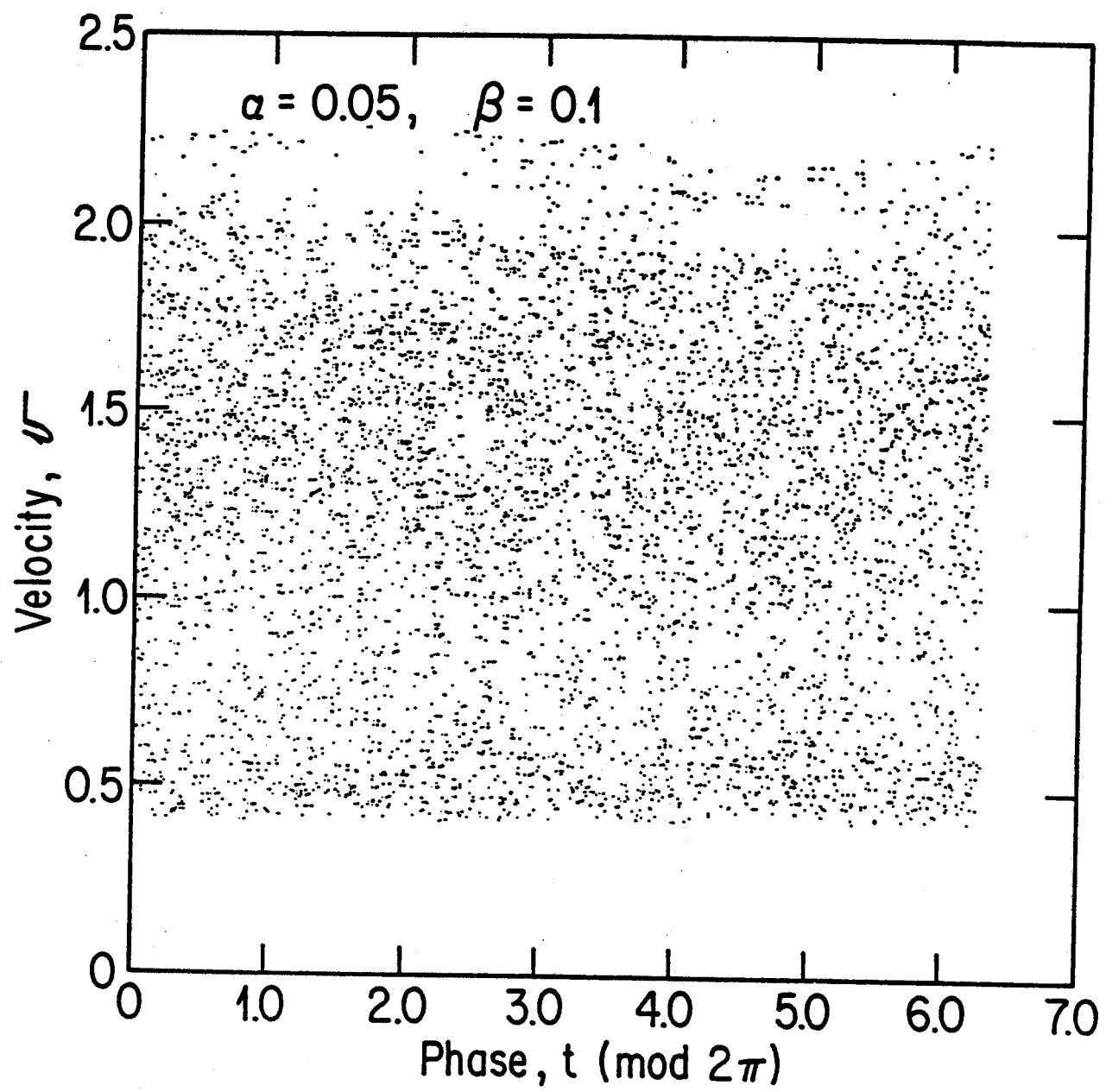
Fig. 7a

Fig. 7b

Fig. 8a

Fig. 8b

Fig. 9

$\beta = 0.1$

$D = \dfrac{\langle \delta v^{-2} \rangle}{2t} \Big|_{\substack{v_0 = 0.8 \\ t = \ell / v_0}}$

$\overline{D}_{QL}$

$\overline{D}$

$D_{QL} = \dfrac{a^2 \pi}{4 \ell \beta v_0} e^{-\dfrac{(1 - 1/v_0)^2}{4\beta}}$

$v_0 = 0.8$

$\sim a^{3/2}$

$\tau_{ac} < \tau_b$ $\tau_{ac} > \tau_b$

Diffusion coefficient

$a = (\omega_b / \omega)^2$
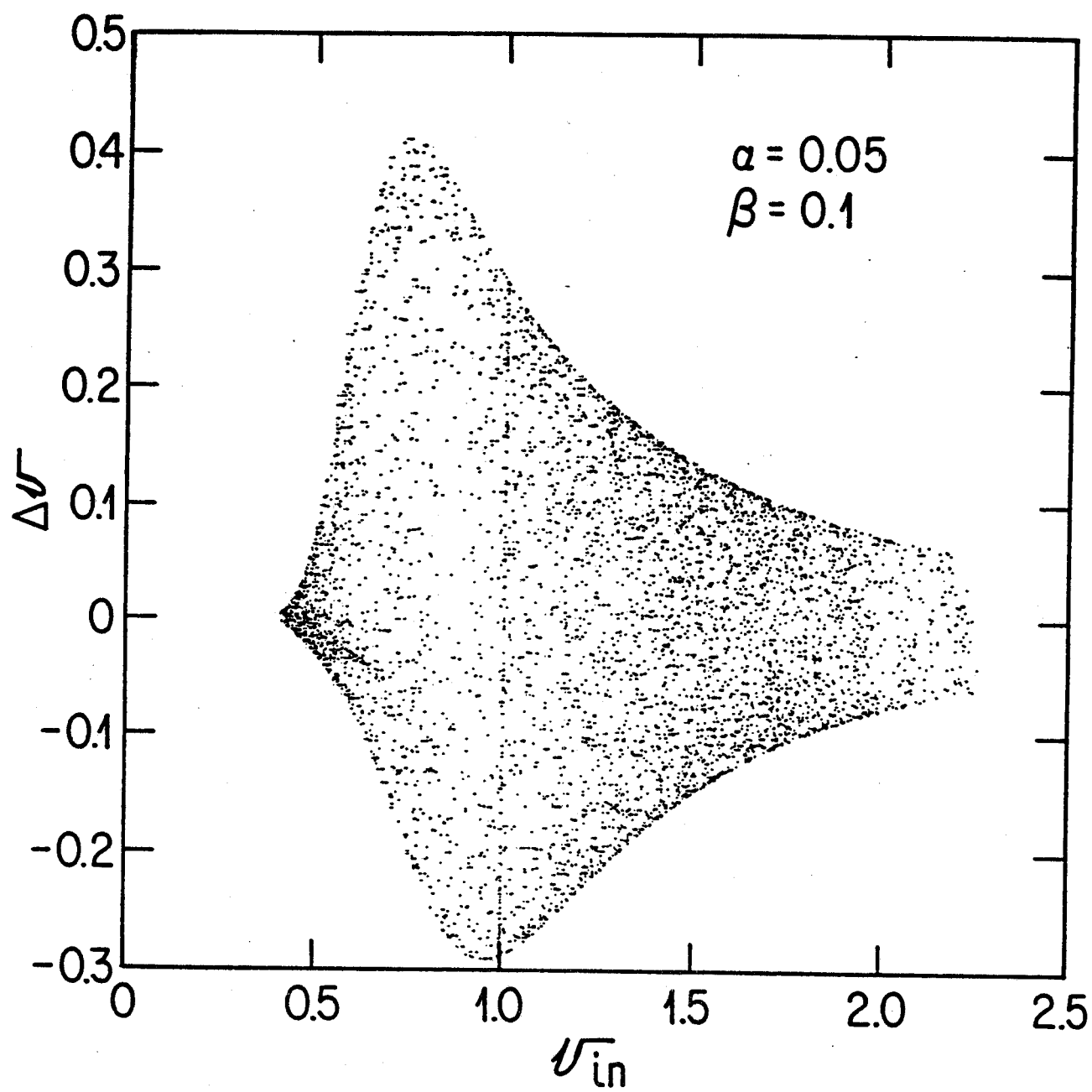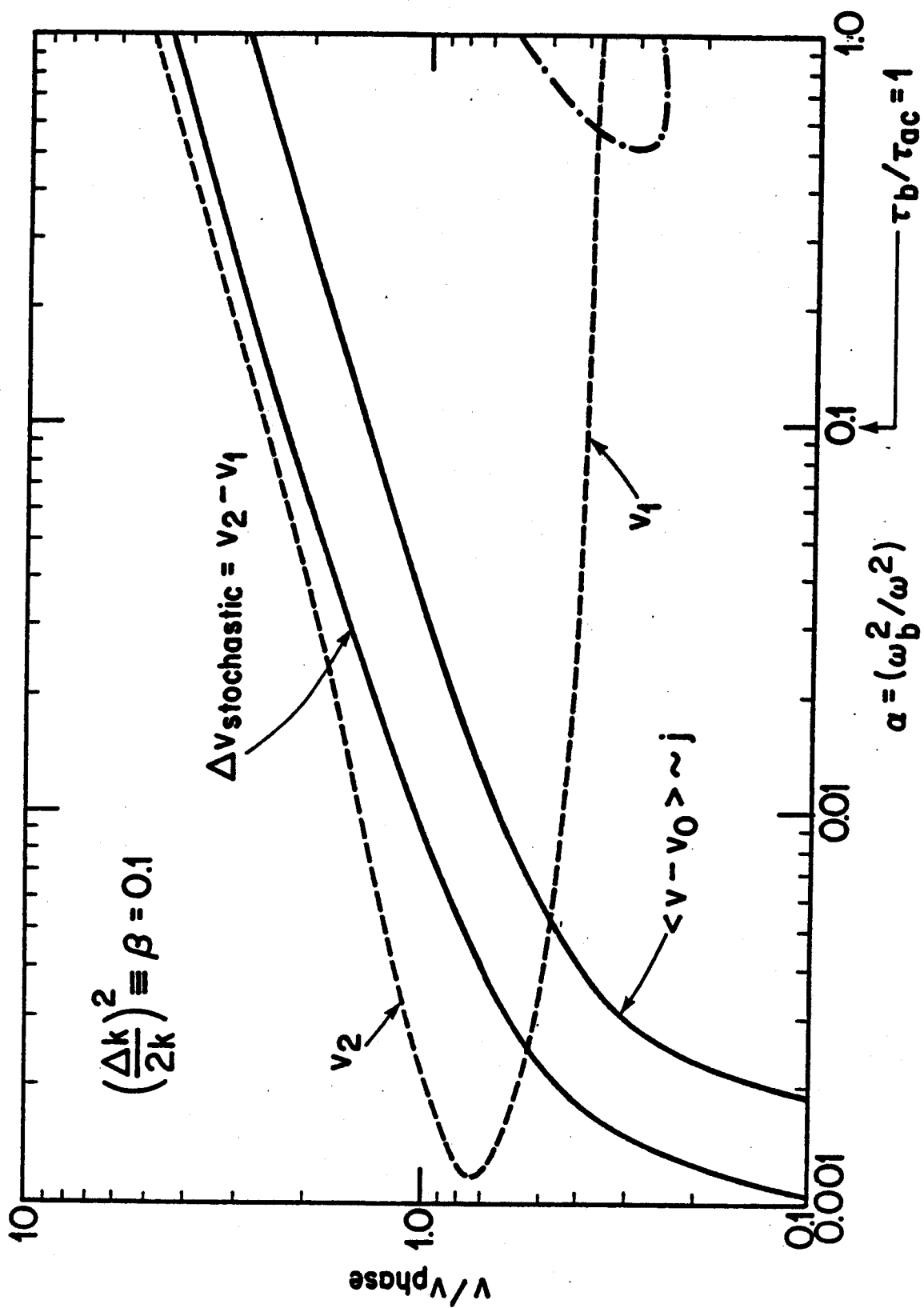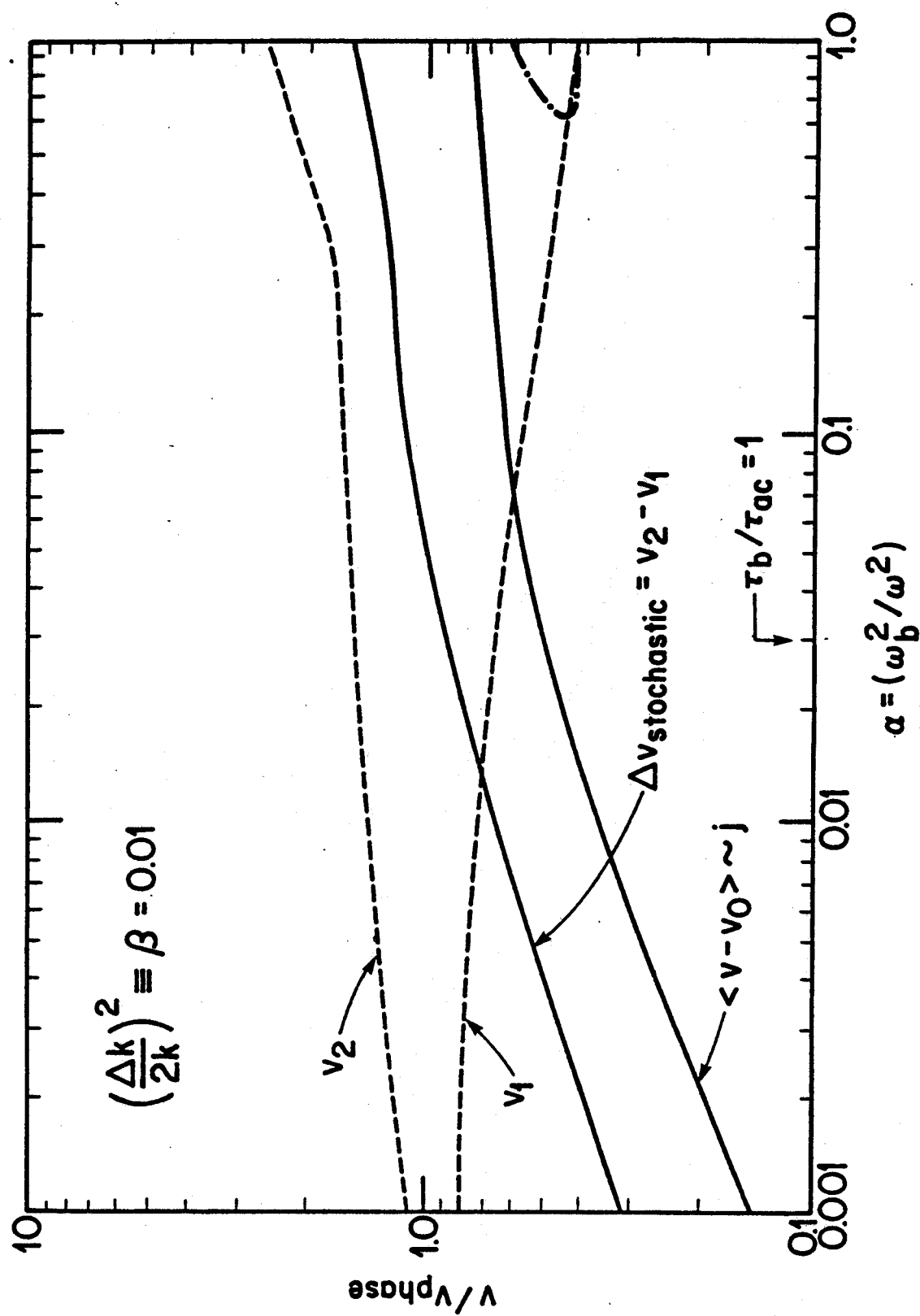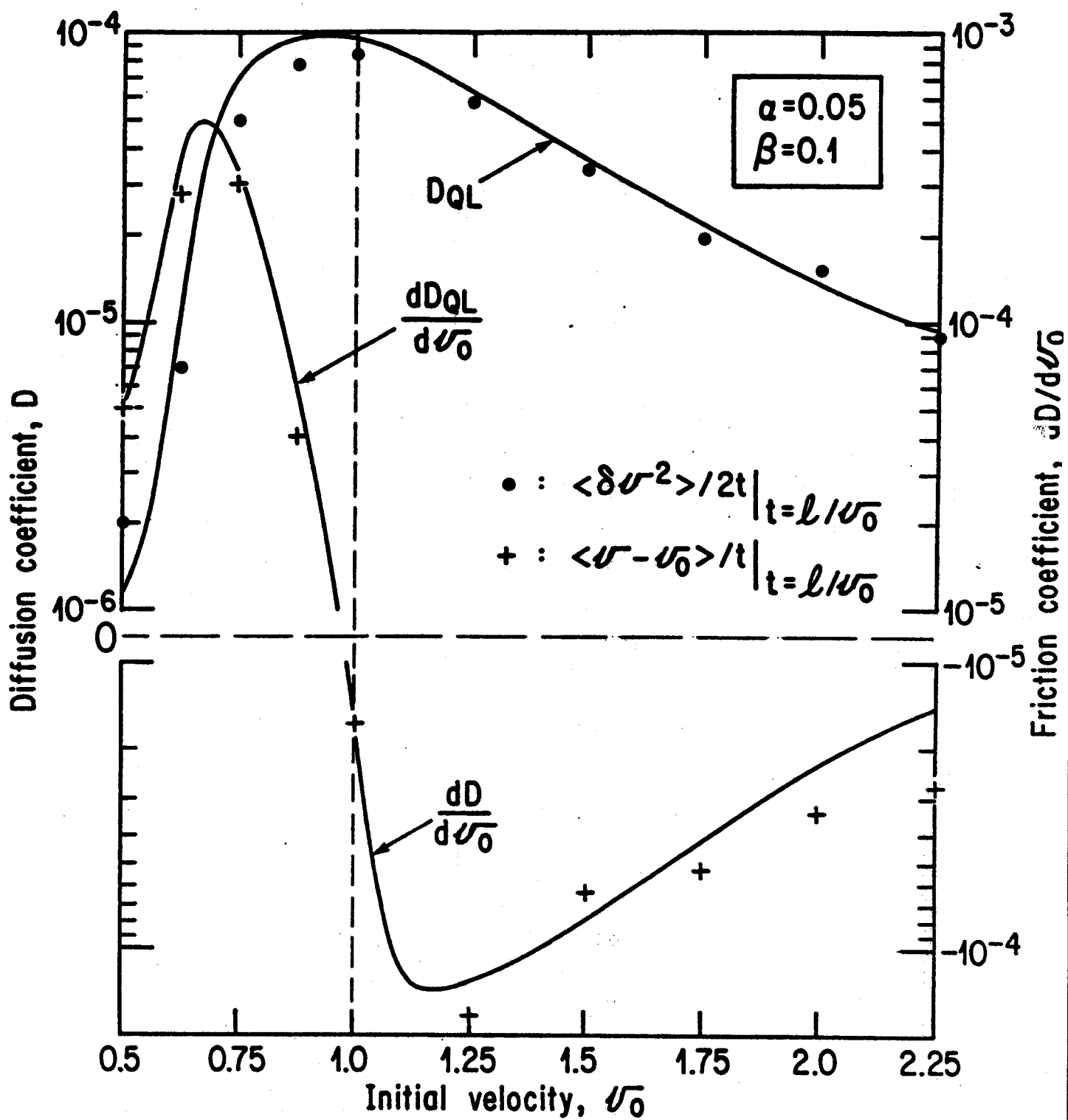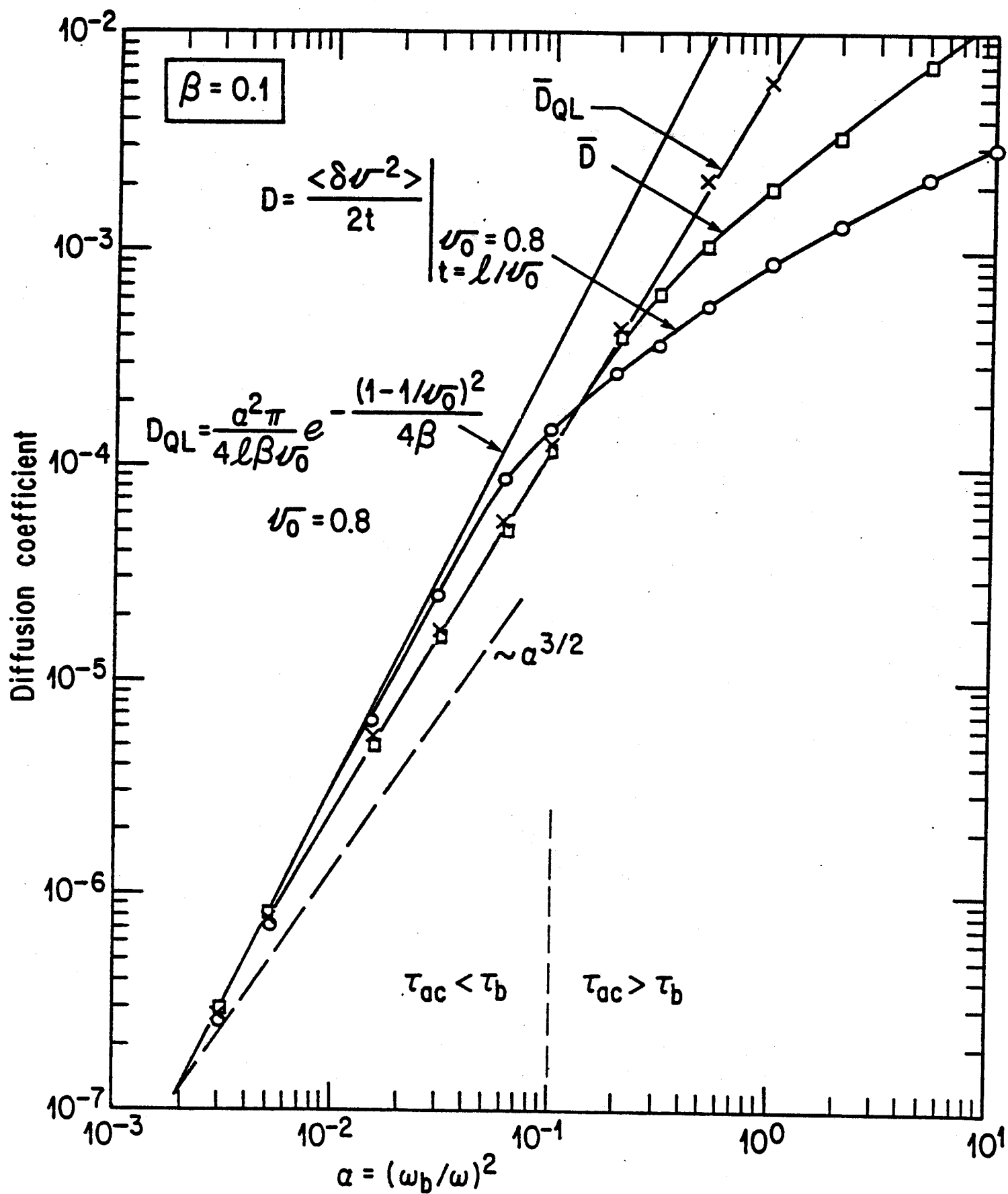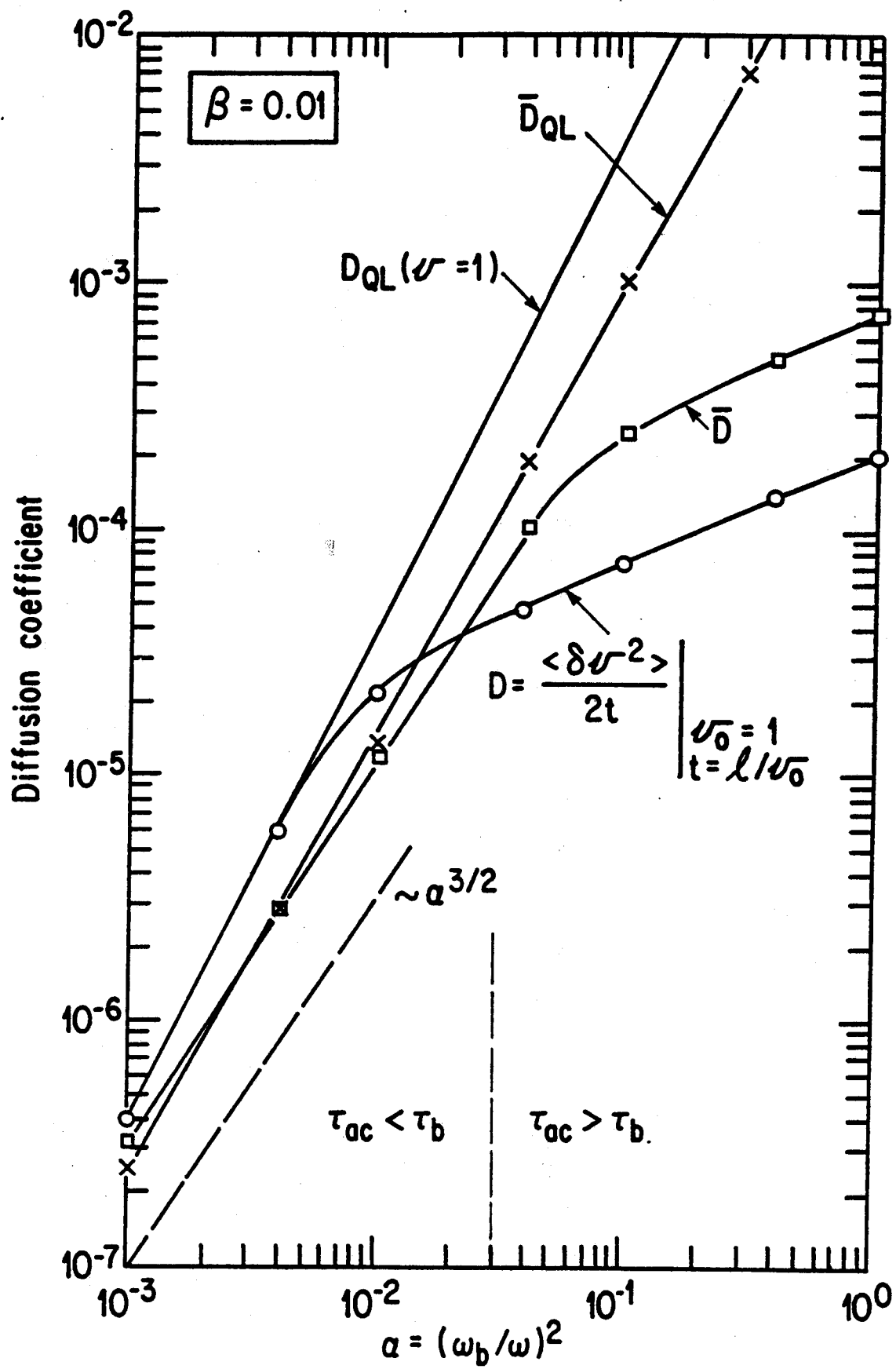
FIG. 10 A

FIG. 10 B
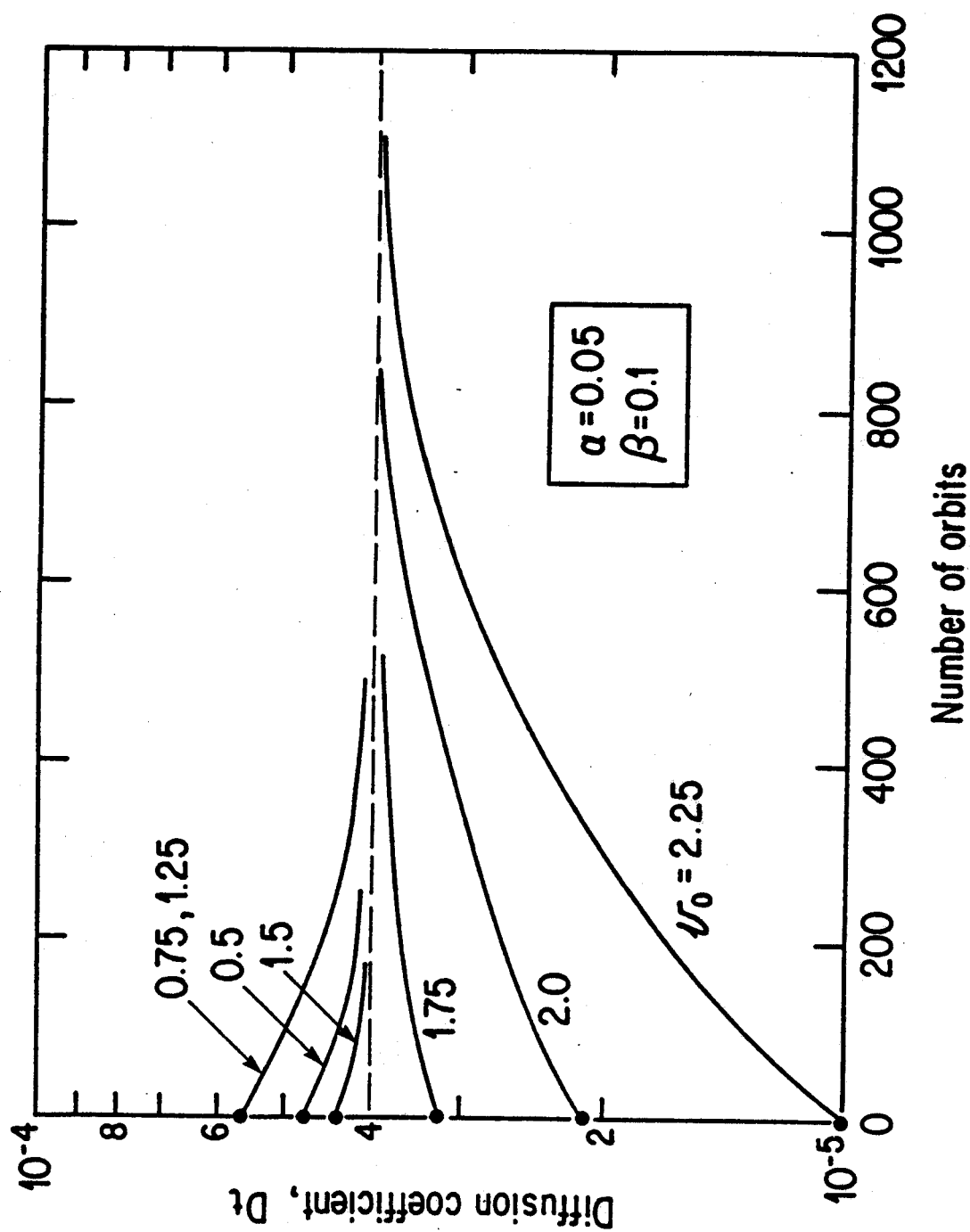
Fig. 11

α = 4,   β = 0.01
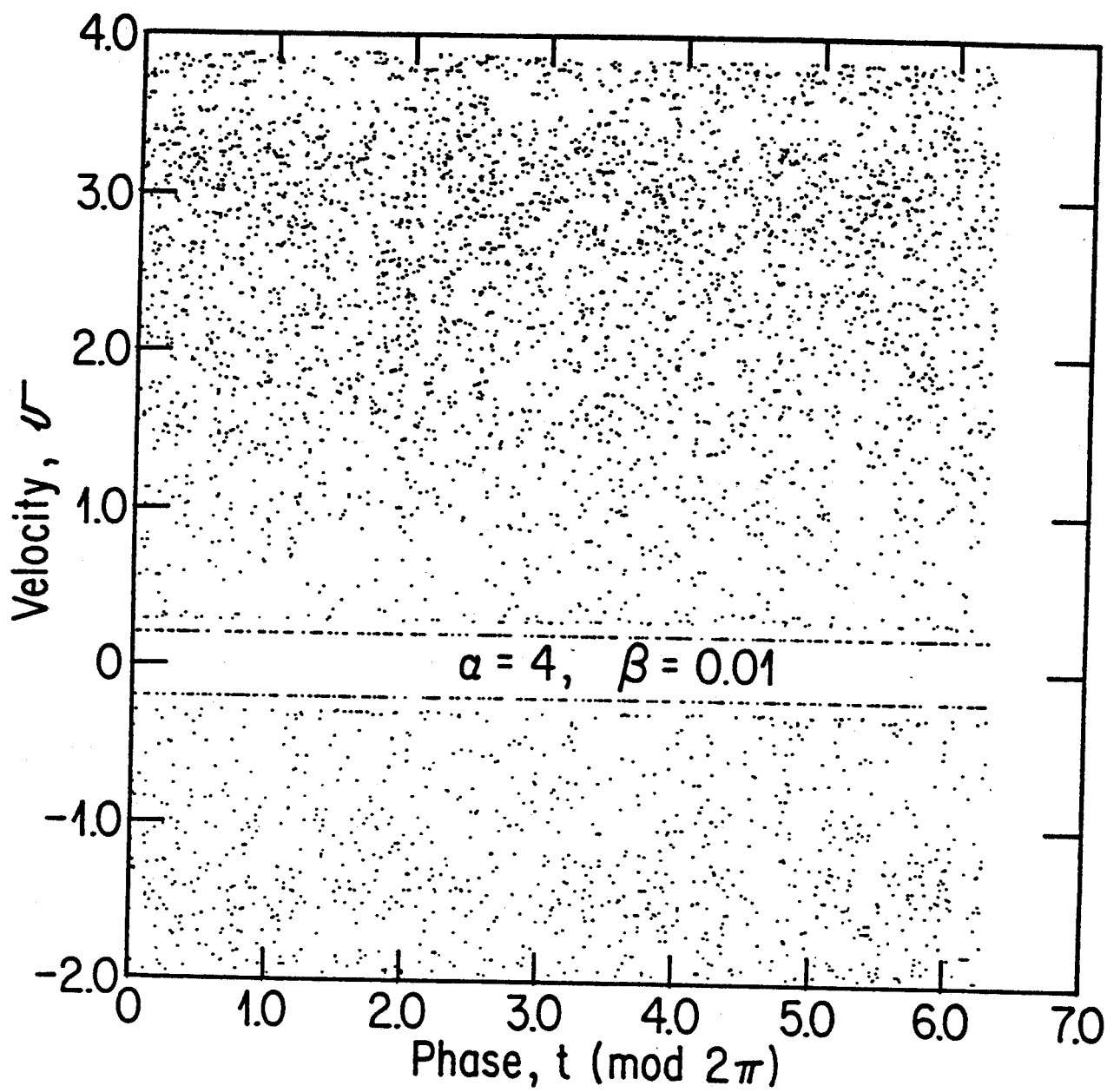
Fig. 12a

Fig. 12b

Fig. 13a

$\alpha = 0.4$
$\beta = 0.01$
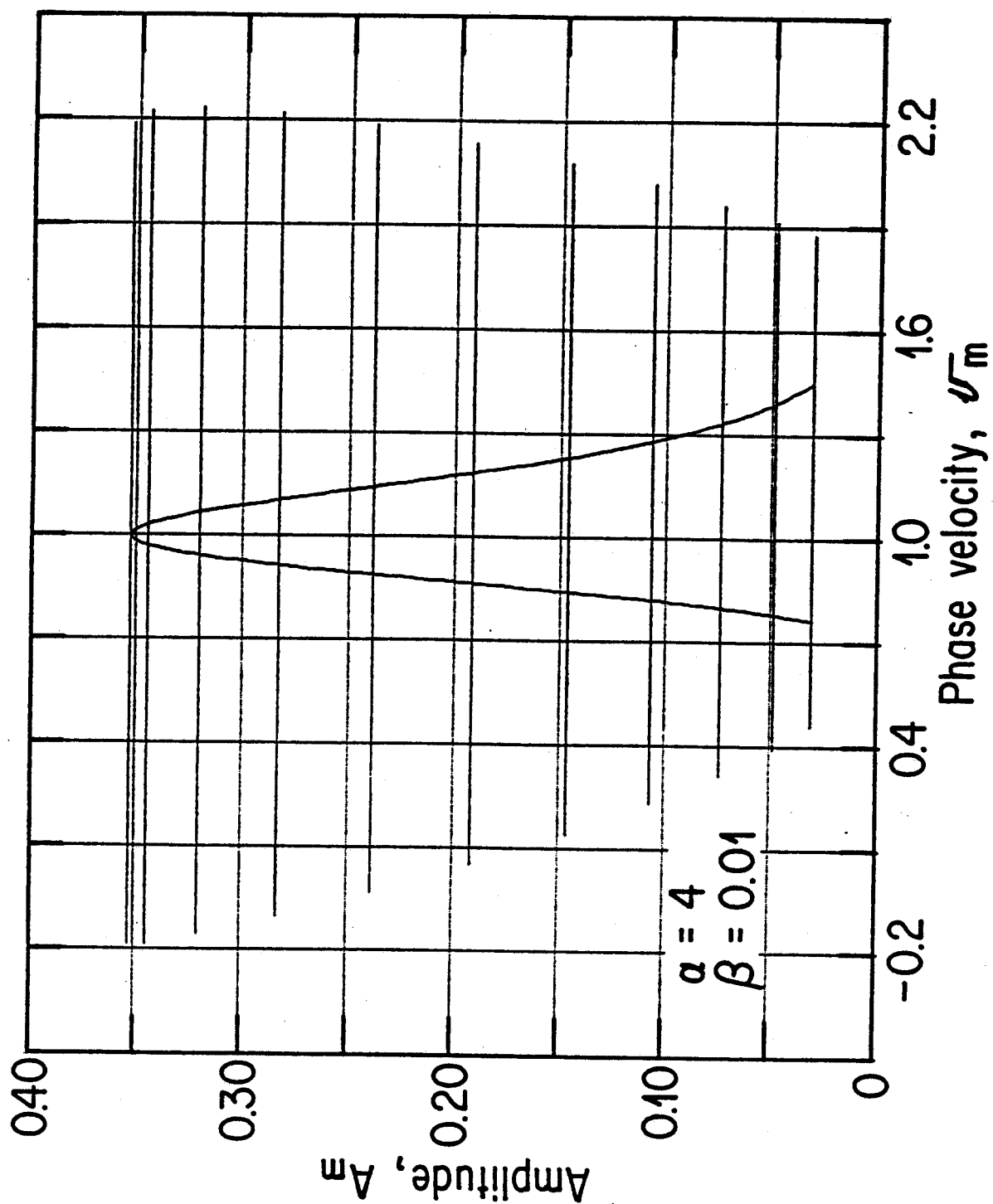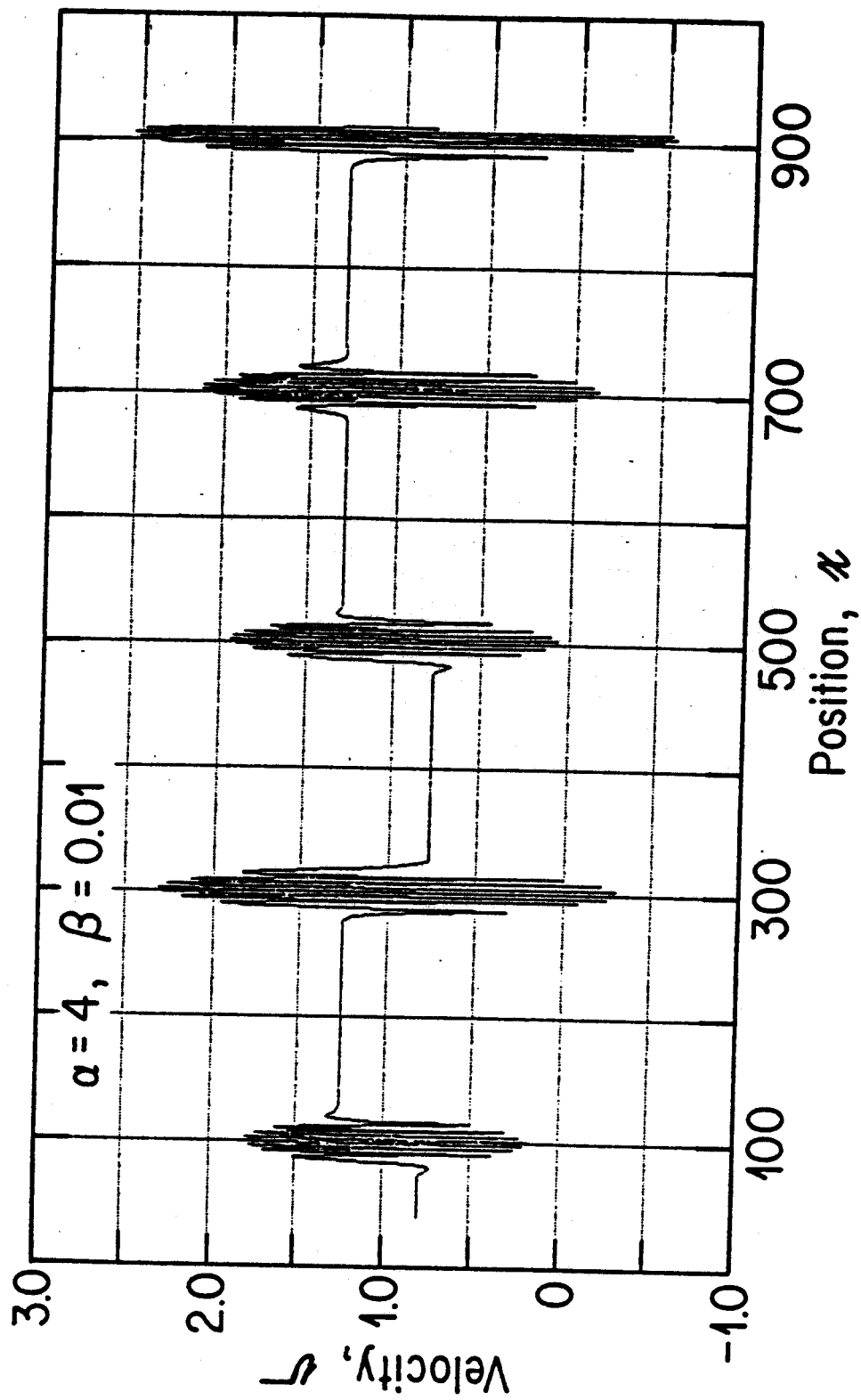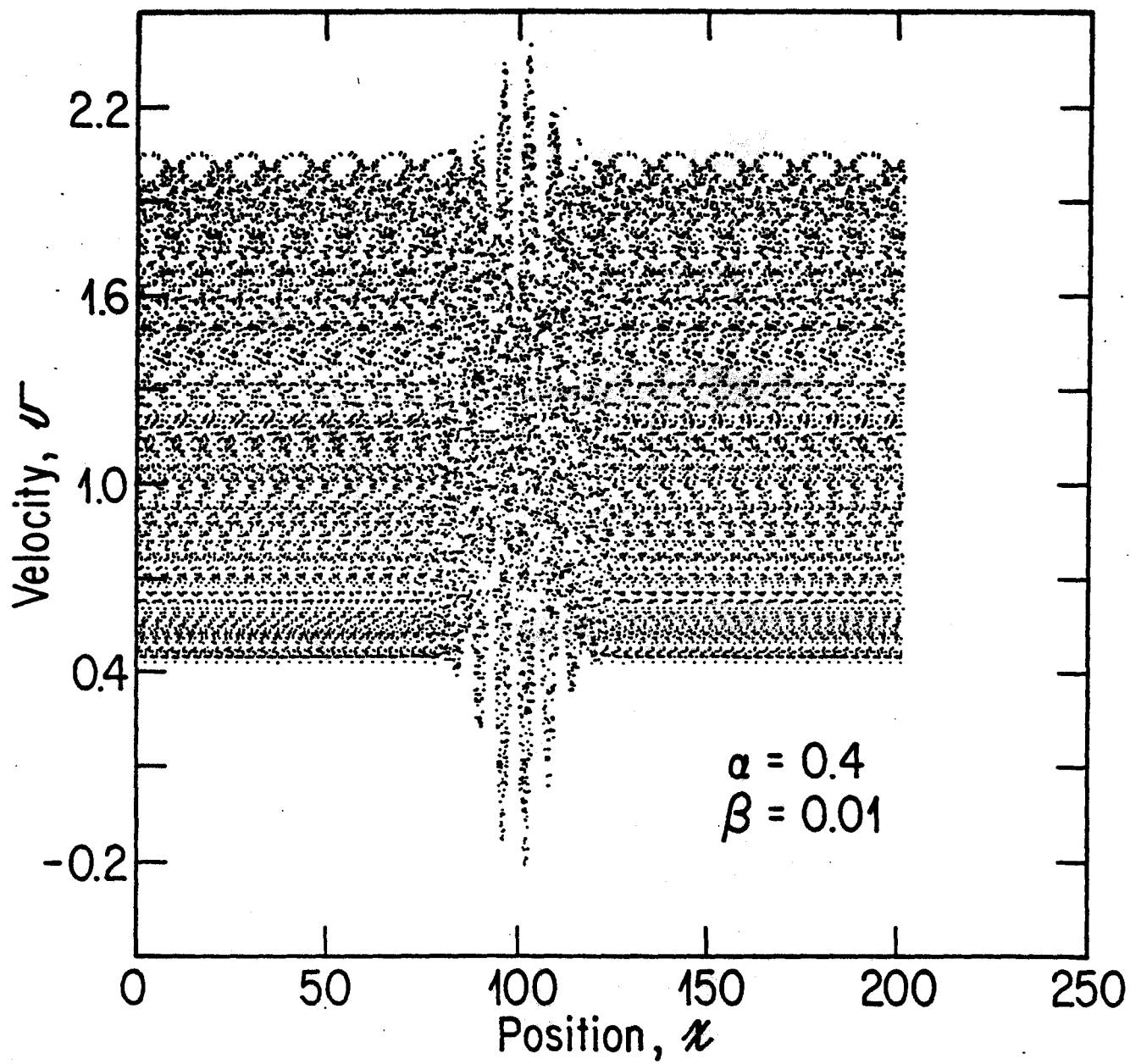
Fig. 13b

Fig. 13c

Fig. 14a

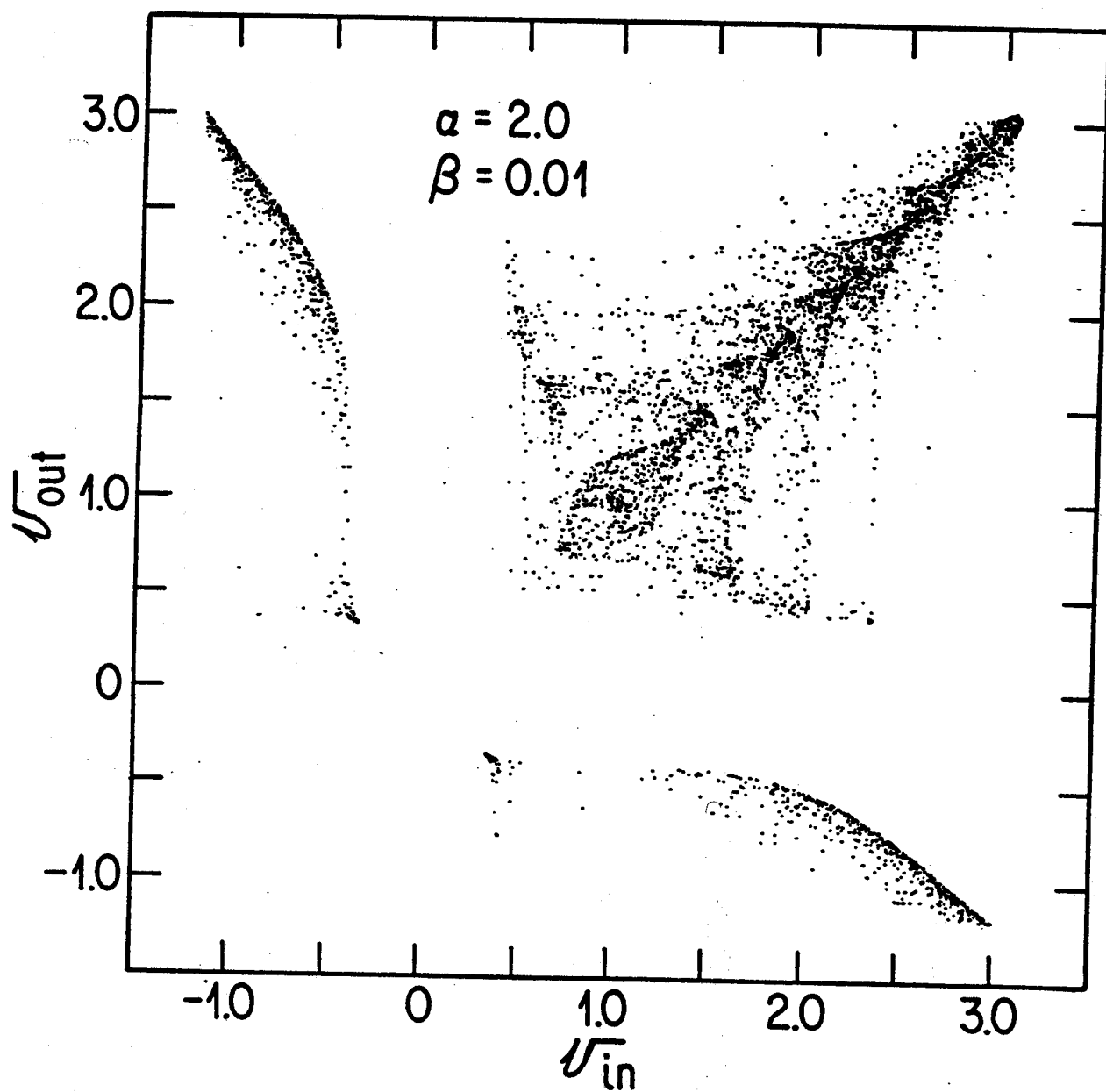$\alpha = 0.5$
$\beta = 0.1$

Fig. 14b

$\alpha = 4$
$\beta = 0.1$
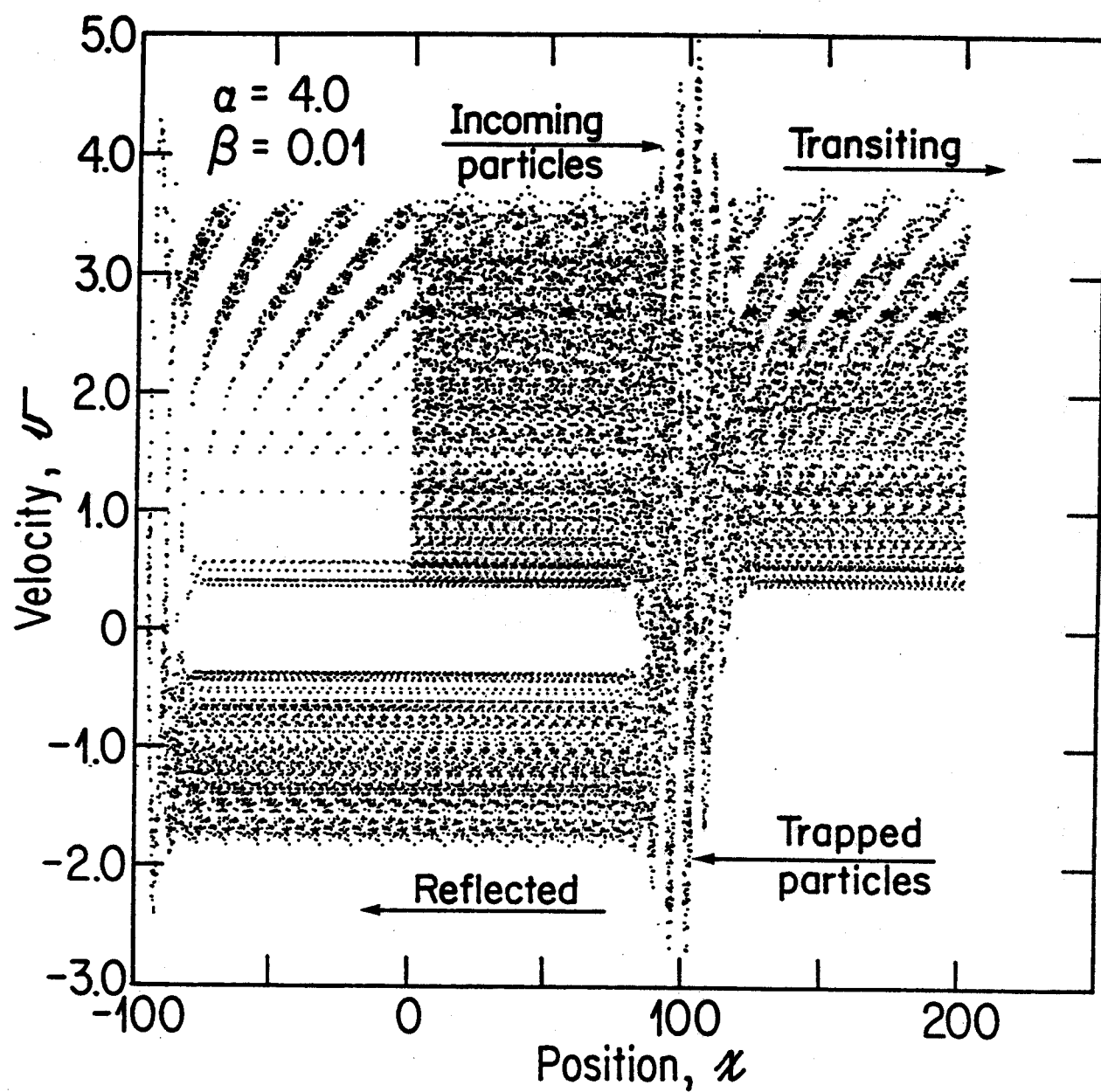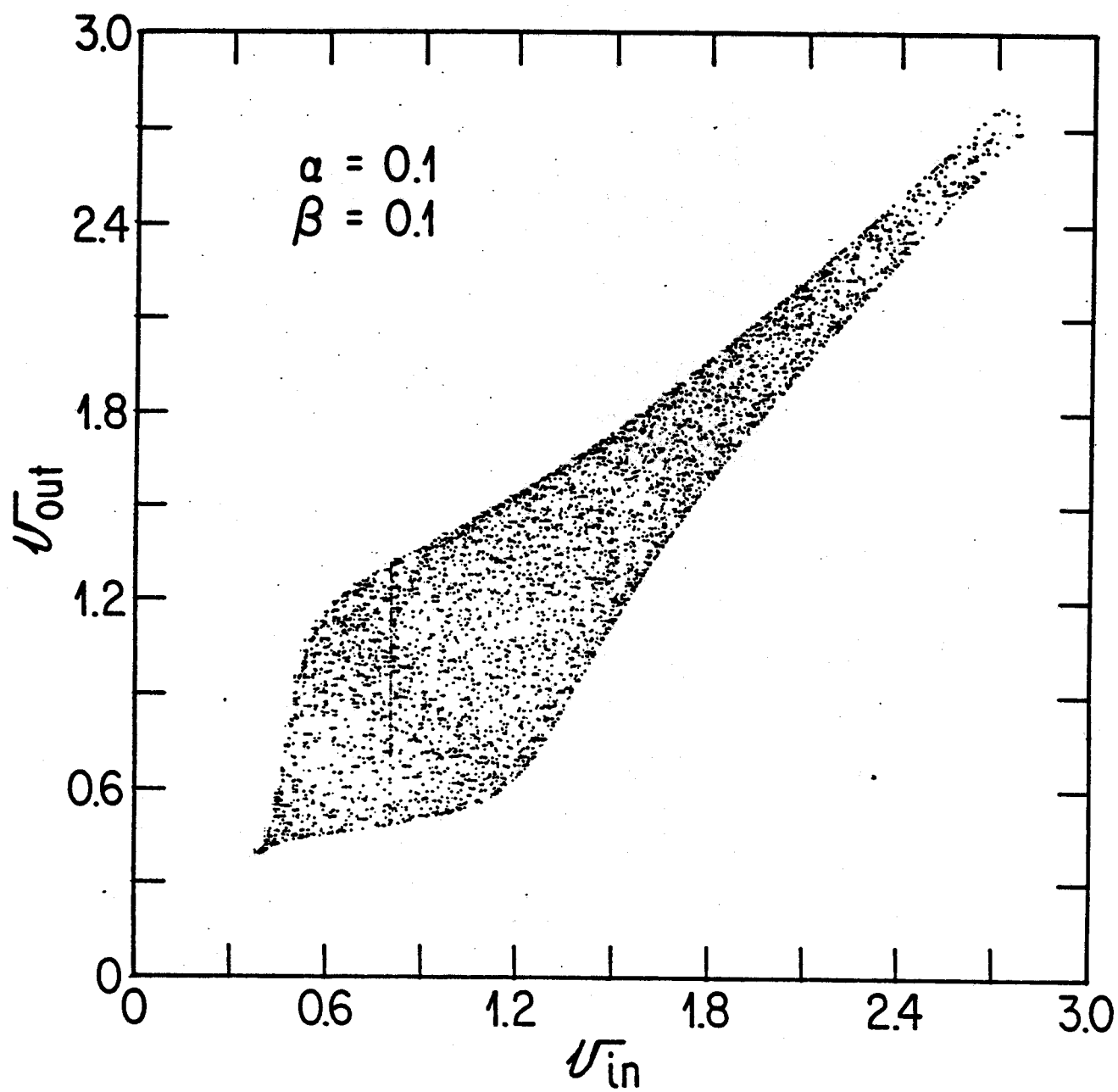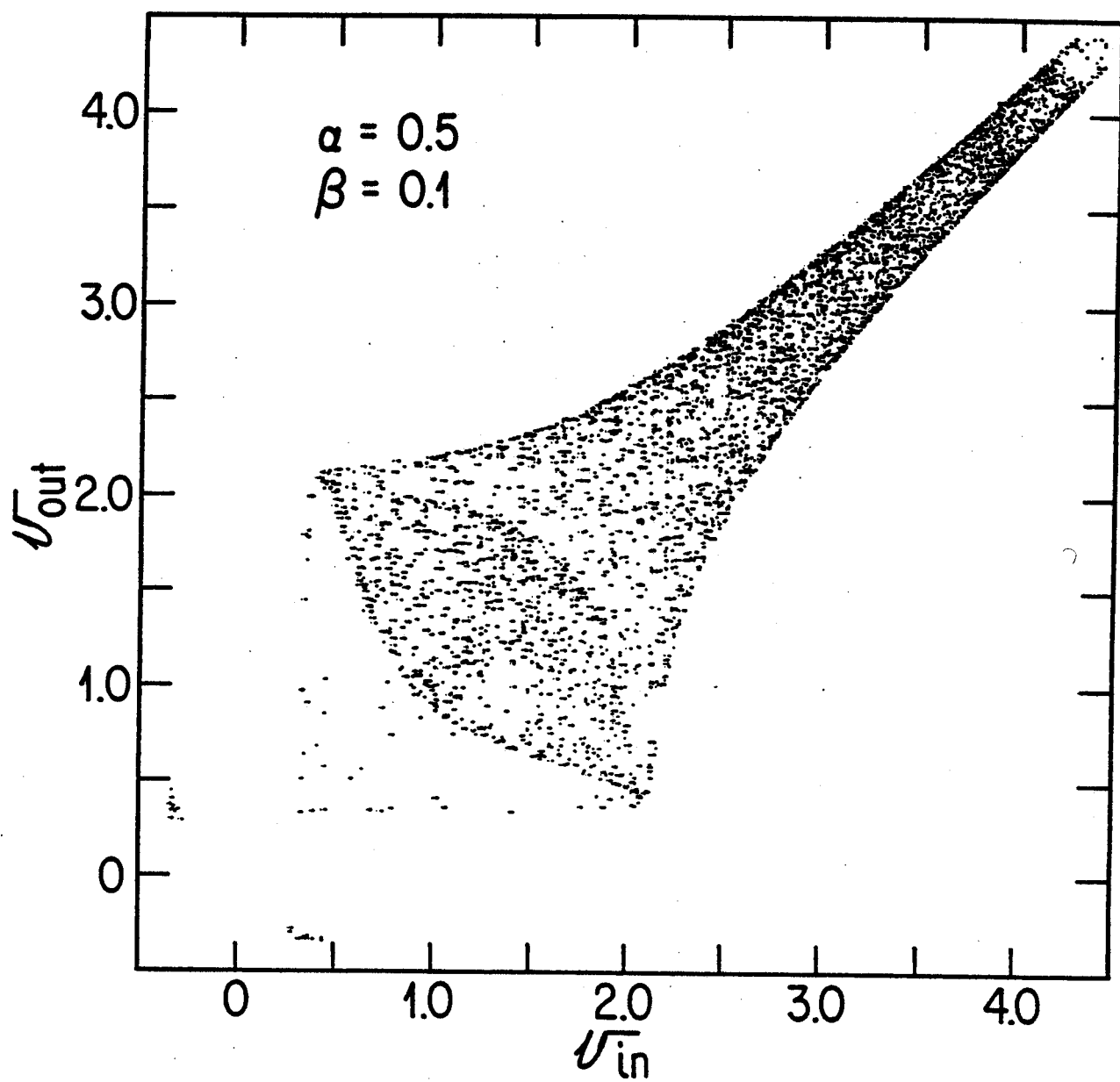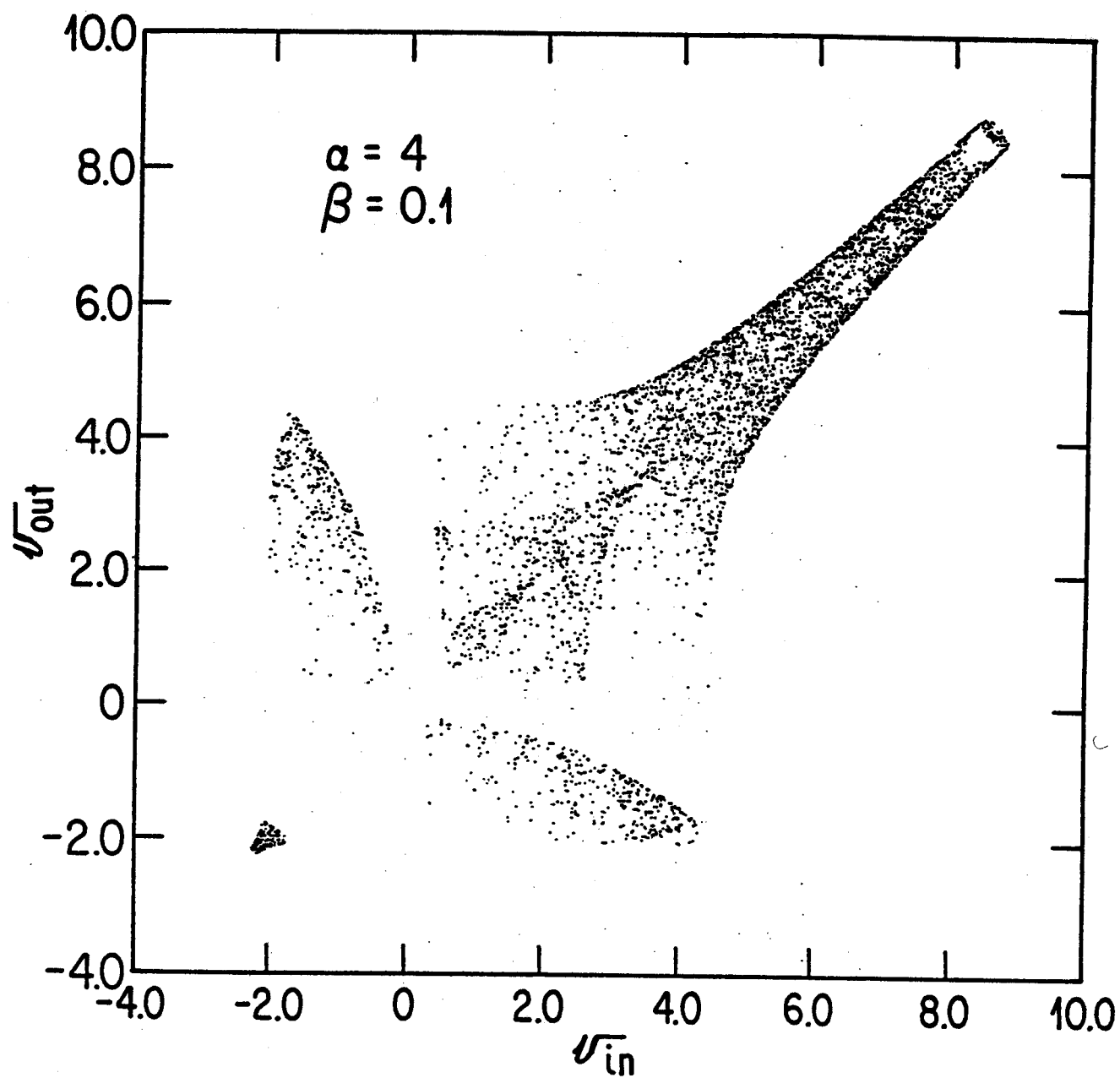
Fig. 14c
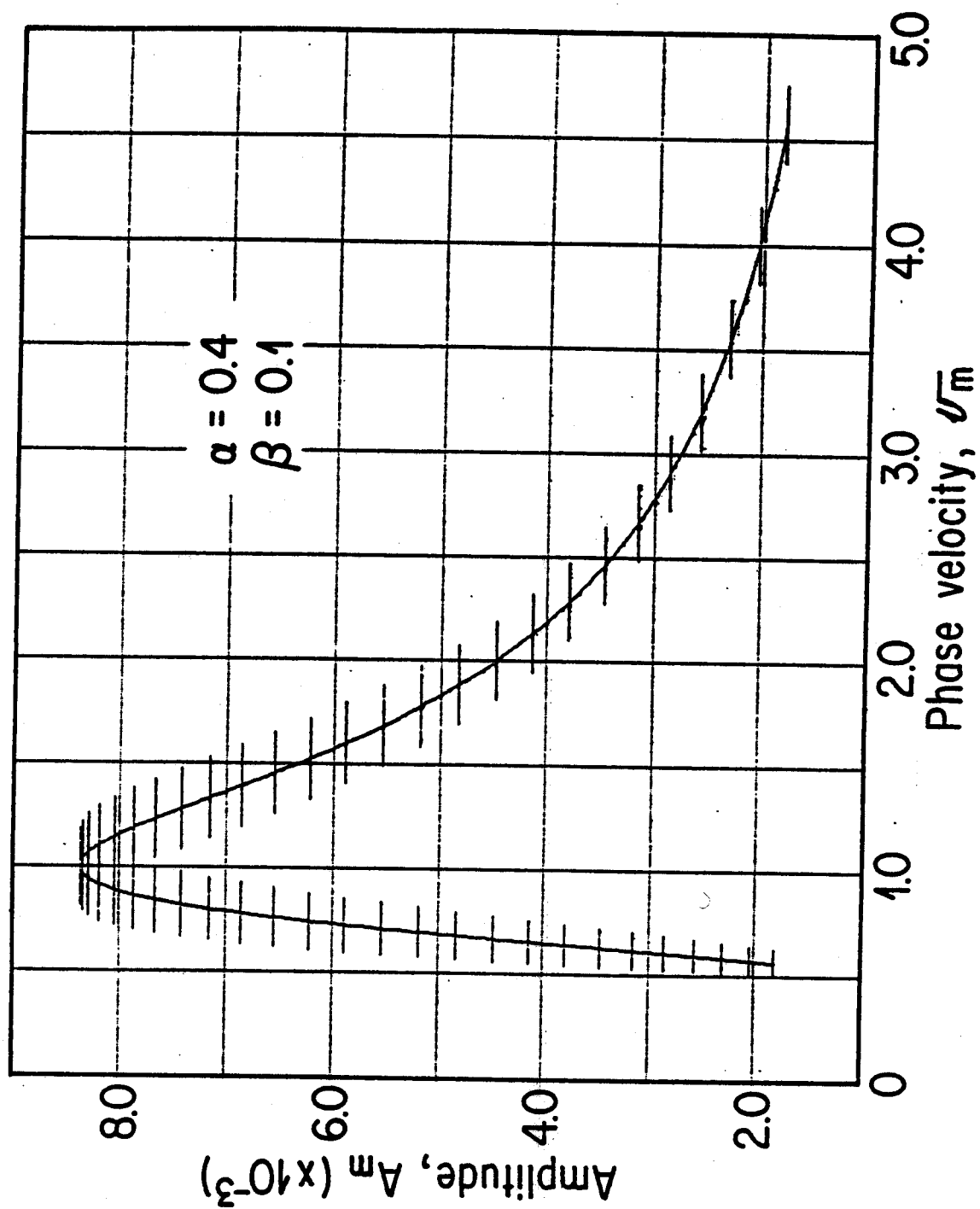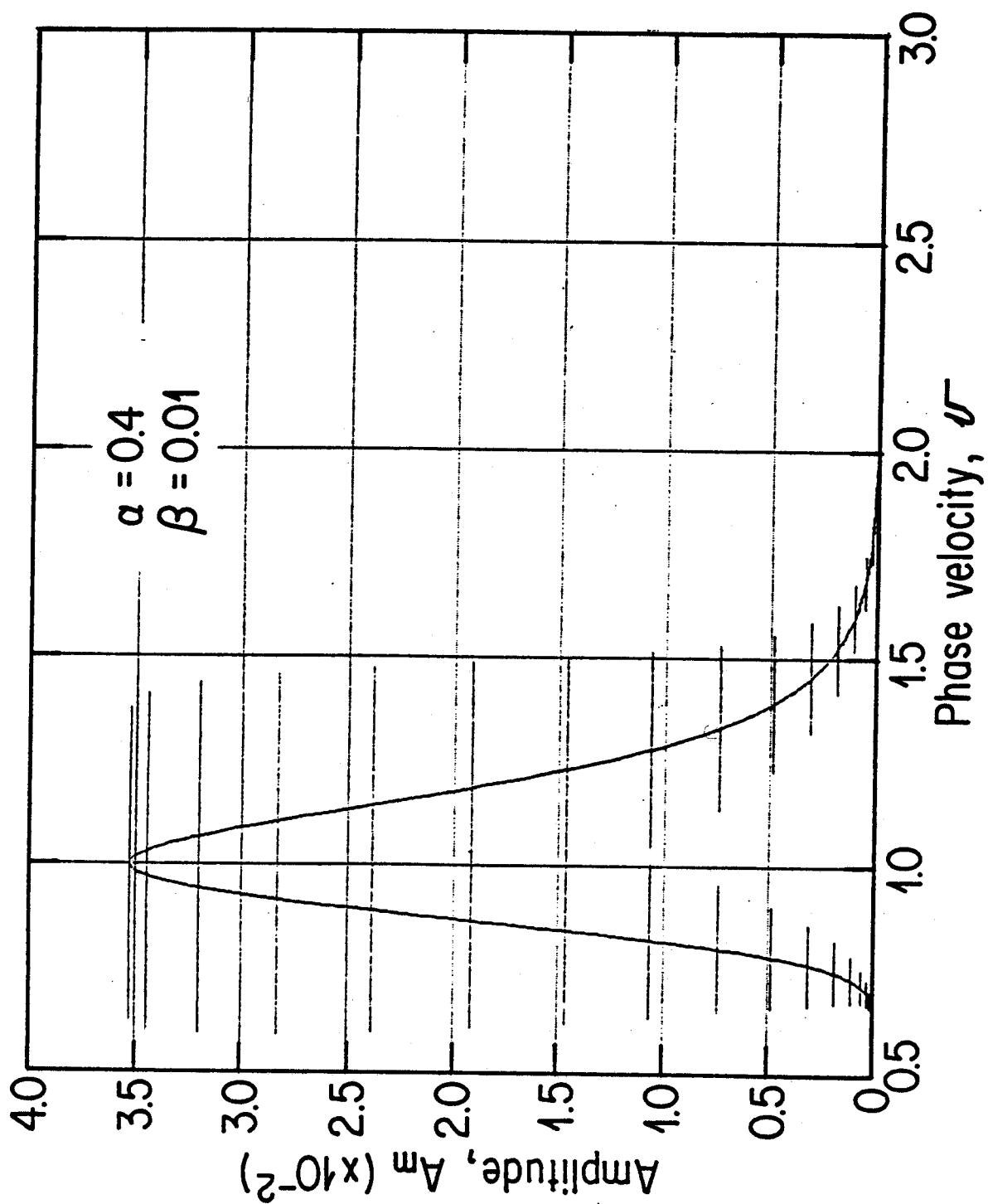
Fig. 15a

Fig. 15b

Fig. 16a

Fig. 16b

FIG. 17